[37] Y.Arai, F.Sudo and T.Emura, "Developments of Time Memory Cell VLSI's." KEK Preprint 93-49, June 1993 H.

[38] Y.Arai, Private communication.

[39] B.Baldin, S.Hansen, R,Li and T.Regan, "Scintillator Counter Trigger Board (Technical description)." D0 Note 2049, February 1994.

[40] R.Goodwin *et al.*, Nuclear Instruments and Methods. A293, pp.125-129, 1990.

[19] V. Sirotenko and S. Striganov, private communication.

[20] B. Baldin *et al.*, "DØ Muon System Front-End Electronics", DØ Note 2370, December 1994.

[21] R. Brock, "DØ Full Scintillator Coverage", Report to a Review Panel, May 1992.

[22] H. Cease *et al.*, "Design description for the CF Bottom B-Layer Scintillation Counter and Support Frame", DØ Note 2731, July 1995.

[23] H. T. Diehl and S.C. Eno *et al.*, "Proposal for Central Muon A-Layer Scintillator Trigger Counters", DØ Note 2213, January 1995.

[24] "DØ-SAMUS background simulations", N. Mokhov, DØ Note 721, Fermilab 1988.

[25] J.M. Butler *et al.*, "Reduction of Tevatron and Main ring induced backgrounds in the DØ detector", FNAL TN-629, Fermilab, 1995.

[26] "Simulation of the test shielding in the DØ forward muon system", S. Striganov, DØ Note 2711, Fermilab 1995.

[27] A. Peisert *et al.*, "Drift and diffusion of electrons in gases: a compilation", Preprint CERN/EP 84-08, Geneva 1984.

[28] D. Green, "DØ pixel array in Run II", DØ note 2018, Fermilab 1994.

[29] G. Alexeev *et al.*, " Studies of stability and systematics of operation of the DELPHI plastic tubes", NIM, A292, 551, 1990.

[30] S. Boyarinov *et al.*, "Neutron and gamma sensitivity of gas detectors", GEM-TN-93-345, SSCL 1993.

[31] B. Baldin *et al.*, "Upgrade of the DØ forward muon system with pixel scintillation counters", DØ note 2358, Fermilab 1994.

[32] Yu. Nikolaev *et al.*, "The efficiency of plastic scintillators to neutrons and gammas", SDC-93-512, SSCL 1993.

[33] S. Abachi *et al.*, "Inclusive muon and b-quark production cross sections in ppbar collisions at sqrt(s)=1.8 TeV", PRL v74, 3548, 1995.

[34] J.A.Holt, D.A.Finley and V.Bharadwaj, "Multibunch Operation in the Tevatron Collider." Fermilab Preprint Conf-93/123, May 1993.

[35] D.Green *et al.*, "Accurate Two-Dimensional Drift Tube Readout Using Time Division and Vernier Pads." Nuclear Instruments and Methods. A256, p.305 ,1987.

[36] M.Fortner *et al.*, "The VME based D0 muon trigger electronics" IEEE Transaction on Nuclear Science. vol. 38, pp.480-485, 1991.

References

[1] De, Draper, Gallas, Kaiser, Li, Perkins, Sawyer, Sosebee, Stephens, White, Ferbel, Grünendahl, Lobkowicz, Yu, Zhu, "Proposal to Upgrade the Intermediate and Forward Regions of the DØ Calorimeter", DØ note 2281.

[2] G. Landsberg, DØ note 2709.

[3] P. Bloom, U.C. Davis, DØ news 250 and 263, UPGRADE folder.

[4] "The DØ Upgrade," DØ Collaboration, DØ Note 2542.

[5] "DØ Muon Chamber Pulse Heights: June 1992 to September 1994 Shutdown," J.M. Butler, DØ Note 2319.

[6] `http://www-d0.fnal.gov/~darien/darien.html`

[7] "Crud Removal from Muon Drift Chamber Wires Using 'Zap' Cleaning," T. Marshall and H. Haggerty, DØ Note 2556.

[8] "The Muon Upgrade Intermediate Eta A-Layer Scintillation Counters," H.T. Diehl *et al.*, DØ Note 2719.

[9] U. Baur and D. Wood in "Report of the *tev_2000* Study Group on Future Electroweak Physics at the Tevatron," D. Amidei and R. Brock (eds.), DØ Note 2589.

[10] "Muon System Pixel Trigger Rates in EF," D. Green, DØ Note 2551.

[11] "High P_t Single Muon Trigger Rate Estimates for the Intermediate Eta Region During Run 2," H.T. Diehl, DØ Note 2605.

[12] H. T. Diehl, "Aggressive Shielding Strategies for the Muon Upgrade", DØ Note 2713, September 1995.

[13] J. M. Butler *et al.*, "Reduction of Tevatron and Main Ring Induced Backgrounds in the DØ Detector", DØ Note 2559, July 1995.

[14] H. T. Diehl *et al.*, "Test of a Polyethylene Shield for the Central Muon A-layer Upgrade", DØ Note 2685, August 1995.

[15] V. Sirotenko, "Shielding for D0 Detector: The First Look", DØ Note 2512, March 1995.

[16] N. V. Mokhov and V. Sirotenko, "Possible Minimal Solutions for DØ Detector Shielding Based on GCALOR and MARS13 Simulations", DØ Note 2601, July 1995.

[17] C. Brown *et al.*, "DØ Muon System with Proportional Drift Chambers", Nuclear Instruments and Methods, A279 (1989), pp. 331-338.

[18] S. Abachi *et al.*, "The DØ Detector", Nuclear Instruments and Methods, A338, (1993) pp. 185.

Level 2 proposal presented here is explicit in its choice of time-frame, signal pathways, and organization. The detailed choices for the elements of the system remain to be frozen, and indeed depend on the rapidly moving electronics industry developments.

All three systems proposed here are now well along in conceptual design, or in many cases into engineering design with prototypes built and tested. Collaborating groups have been identified who have carried the R&D, tests in the Run I environment, and prototype building. The time scale for building these systems is such that full scale fabrication needs to begin in this year.

We believe that the forward preshower, the muon trigger and coordinate measuring detectors, and the Level 2 trigger system have all conformed to the approved goals for the DØ upgrade, and that the present proposal represents a controlled and achievable completion of the baseline design for Run II operation, when the Main Injector starts operation in 1999. We recognize that the cost of the full baseline design, including these final elements, exceeds the funding advice given by the Laboratory, but are committed to find the external sources of funding and/or discuss possible staging options to bring the full detector into operation as rapidly as possible.

We request positive recommendation from the PAC for these systems, and approval for their fabrication from the Laboratory.

5 Summary

In this document, we have proposed three specific systems to complete the baseline DØ upgraded detector for operation in Run II, starting in mid-1999. All have been proposed and presented in earlier reviews, but have not heretofore received full approval.

We emphasize that none of these represents a scope increase of the DØ upgraded detector. The preshower concept was introduced in the original 1990 proposal as necessary to regain the electron trigger capability and good offline identification of electrons following the removal of the Run I transition radiation detector and drift chamber ionization measurements and the introduction of the added material of the solenoid coil. Earlier versions of the DØ upgrade proposal had tracking chambers extending to $|\eta| = 3$, and so the possibility for useful trigger information on forward electrons could be hoped for from these detectors. With the decision to remove the forward tracking for cost-control reasons, the forward preshower detector became imperative to achieve the approved goal of adequate trigger power and offline electron identification.

From the start, the upgraded muon system has included new triggering devices to enable muon triggers at the high luminosity and short bunch crossing times. This portion of the proposal was originally approved in 1991. The proposal presented here gives specific realization for these triggering elements. What is new in the past year is the understanding that the existing muon proportional drift tube chambers (WAMUS) suffer from a persistent radiation damage problem. This problem was identified in winter 1994-95, and a solution ('zapping') found to cure it was implemented in the January 1995 shutdown. However in Spring 1995, it was determined that the fix was temporary and the chambers in high radiation areas needed periodic re-zapping. The aging problem has been quantified and documented, and presented to the PAC in its June and October 1995 meetings. With the information obtained on the aging rates, and thus the intervals at which zapping would be needed, it became apparent that the WAMUS chambers at $|\eta > 1|$ could not be operated in Run II. In summer 1995, the DØ collaboration proceeded to re-optimize the whole muon detection scheme for $|\eta| > 1$ with the understanding that the coordinate-measuring chambers would need to be replaced. This overall re-optimization has led to the present proposal, and in many ways gives a superior muon triggering and measurement system, better coordinated with the upgraded central tracking systems already approved. The present proposed muon upgrade thus does not represent any modification of the functional scope for the muon system. In fact, the decision to remove the small angle SAMUS chambers to permit shielding installation is a reduction in scope.

Finally, we have presented our plan for the Level 2 trigger system, recognized since 1990 as necessary to handle the factor of ten increase in collision rate. We have noted that the increase in rate cannot be simply handled by cranking up the thresholds for triggers in Run II; the physics issues that motivate our program are largely based on the study of objects (the top quark, W and Z bosons, the b-quark hadrons) whose masses are fixed and thus determine the thresholds for recognizing their decay objects. The increase in maximum luminosity to be expected during Run II (from 1 to $2\times10^{32}\mathrm{cm}^{-2}\mathrm{s}^{-1}$) has generally not affected our detector upgrade designs. But for the trigger, it simply dictates that an extra factor of more than two in power is necessary. (More than a factor of two, because our experience is that most trigger cross-sections actually increase with increasing luminosity and event pile-up.) The provide intuition and extremely rapid turnaround time, but are restricted to exponential distributions for processing time. These simulations were the first to point out the need for 16 L2 buffers. At the opposite end of the spectrum are full-scale RESQ simulations which internally incorporate a mixture of analytical and Monte Carlo methods. Sometimes this "black box" had limitations in incorporating particular important details of our system because we have no access to source code. In between are direct custom-written Monte Carlo simulations, which allow full flexibility in time distributions and details, but which typically are capable of modelling only pieces of the full system. All three approaches have been and are being used for simulations.

An example of the kind of study done is given in Fig. 20. Here we consider in RESQ a part of the L2 chain: a preprocessor followed by a single, input buffered, global processor. This arrangement might be thought of as a stochastic pipeline, as the processing time of each stage of the chain is allowed to vary. Events arrive at 10 kHz. We vary the mean preprocessor time while the global processor mean time is held fixed at 75 μs. The cutoff at 125 μs noted in the figure refers to the fact that we force a decision in the global processor and transfer to L3 at this cutoff time, thereby limiting the decision time. There are 16 input buffers in front of the preprocessor, and we idealize the connection to the global processor by an infinite set of buffers, but restrict the total number of events anywhere in the chain to 16. The figure shows the expected rapid increase of deadtime as the mean preprocessing time approaches the mean event arrival spacing of 100 μsec. The deadtime approaches zero at 50 μseconds, because this is the fixed latency used in this model and corresponds to the case where the algorithm takes no time to execute.

These simulations of the trigger system are critical for developing a viable design of the complete trigger. They are the crucial information needed to balance the number of L2 buffers, the number of L2 trigger nodes and the average L2 trigger decision time. Based on these simulations we are designing the L3 part of the trigger in such a way that it can act as a buffer for events when the L2 system has exceeded some cutoff time for a particular event. In this case we anticipate a "Maybe" signal from L2. After receiving this signal, the front end system considers the event as passed by L2 and transfers it to L3, thereby freeing up L2 buffers. Because the L2 accept/reject information has to be in the same sequence as the L1 accepts, this also frees up L2 processors that have been waiting with their decisions ready. L3 stores the event that exceeded the time cutoff in a special input buffer, while other events are passed or rejected. Once the L2 node for this event finishes, it communicates this information to L3, which then either keeps the event for further processing or simply dumps it. Of course, the fraction of events allowed to exceed the cutoff in L2 has to be kept on the order of a few percent. This part of the design is currently under active study.

The L2 system design will evolve in the next year, so the present estimate of the system costs are not detailed. The estimated M&S cost for the full L2 system is $1.6M.

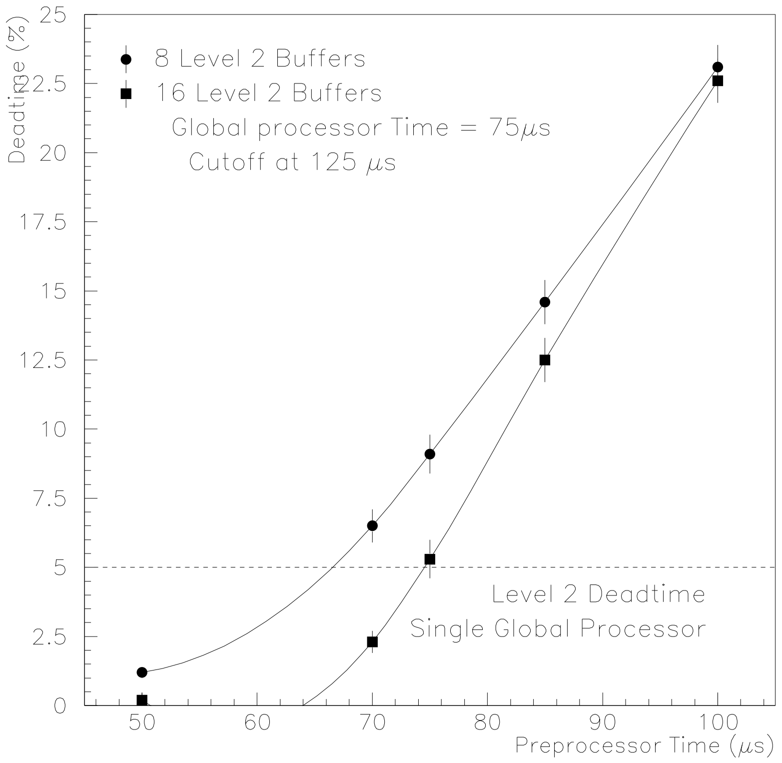

Figure 20: Deadtime in L2 system as a function of preprocessor time. Preprocessor time includes transfer time and algorithm execution time.

are needed to store events. Presently we anticipate having a buffer in every front-end system which can hold 16 events that have passed L1 and are waiting for their L2 decision. These buffers are referred to as the "L2 buffers". It takes some time to transfer the events into the preprocessors and this time is referred to as latency time. It is typically of the order of 25–50 μs and is based on measurements in the current Level 1.5 system. The mean algorithm execution time in the preprocessors is order 25–30μs and again is based on measurements of the execution time of the electron algorithm in the current Level 1.5 C40 DSP's. The total time required for the preprocessor to complete its task is the sum of the two. The transfer time is fixed, but the algorithm execution time is described by a distribution, due to the variation from event to event in the number of candidates to be compiled, with a mean as quoted above. We expect that the algorithm used in the preprocessors can be standardized to minimize the variation in the time required for the list-making tasks.

The input to the global processor farm , through the data switch, will again contain a number of event buffers. The maximum at this point is 16 and some of this functionality may be provided by the data switch. The processing time in the global processors is taken to be exponential with a maximum *mean* time of order 200 μs. Our examination of typical L2 algorithms and experience with the Run I Level 1.5 trigger shows that this expectation is reasonable.

The design is proceeding hand-in-hand with extensive queuing theory simulations. Several models are used to provide cross checks. Simple analytical models of simple queues control their actions are downloaded into the processors. The flexibility of the scripts and the ability to adjust them easily are prime features of this system. It allows us to accommodate easily to the expected increase in luminosity and possible changes in our physics menu. This has proven to be extremely useful during Run I, where we covered a large range of instantaneous luminosities as well as a large variety of physics topics. At the global processor level one has to strike a compromise between flexibility and decision time. The average decision time at this stage of the system should be on the order of a few hundred μs for the deadtime to be kept low.

We take as an example of a global algorithm the L2 central electron identification. At L1 a typical electron candidate is required to have an energy in an electromagnetic tower of the calorimeter with $E_T > 10$ GeV. In addition, requiring a track at L1 anywhere in the central detector, with $P_T > 10$ GeV/c and electron-like energy deposition in the preshower, reduces the rate of the calorimeter trigger by a factor of 3. We also anticipate obtaining information on the z coordinate from the track trigger for use in L2. Feeding this information into L2 and requiring a match in ϕ and z between calorimeter and tracker reduces the rate by another factor of 3. This rejection is independent of luminosity. Our understanding of the time required for such an algorithm, based on the current performance of the Run I Level 1.5 processors and improvements in hardware performance, suggests that the algorithm can be completed comfortably within 200 μs.

As indicated in Fig. 19, we expect that several global L2 processors will be needed to achieve the required deadtime. This number will be determined through overall system optimization, and will depend upon the maximum luminosity expected in any given run period. In deriving the cost estimate, we have assumed four global processors, with suitable buffering at their inputs.

At this point the hardware to be used for the components of the L2 system is not fully specified, but will be primarily driven by the limits on the decision times that are allowed. From the experience with the Level 1.5 trigger in Run I, we anticipate that the algorithms in the preprocessors and global processors can be executed by software in fast processors. These could either be VME mounted RISC-based units or digital signal processors (DSP's). The difference between the two is essentially in the balance of data transfer vs. number of instructions executed. DSP's are better in data transfer, whereas RISC processors are faster in execution of instructions. At this point we have experience with DSP's in our Run I Level 1.5 trigger, but not with RISC processors. Because of tighter constraints on decision time for the preprocessors they may have to be dedicated/custom made hardware devices, but at this point we would like to keep as much commonality in the system as possible. For that reason we prefer to use the same or a similar hardware solution for the global as well as preprocessors.

4.3 Timing studies of the L2 system

A major requirement of the L2 system is to introduce a minimal amount of deadtime (<1%) in the trigger. To verify this we have simulated the timing behavior of the system for several conditions. In the following we describe the assumptions made for the simulations and the techniques used to simulate the system.

To keep events flowing through the complete trigger and data acquisition system, buffers

L2 Architecture

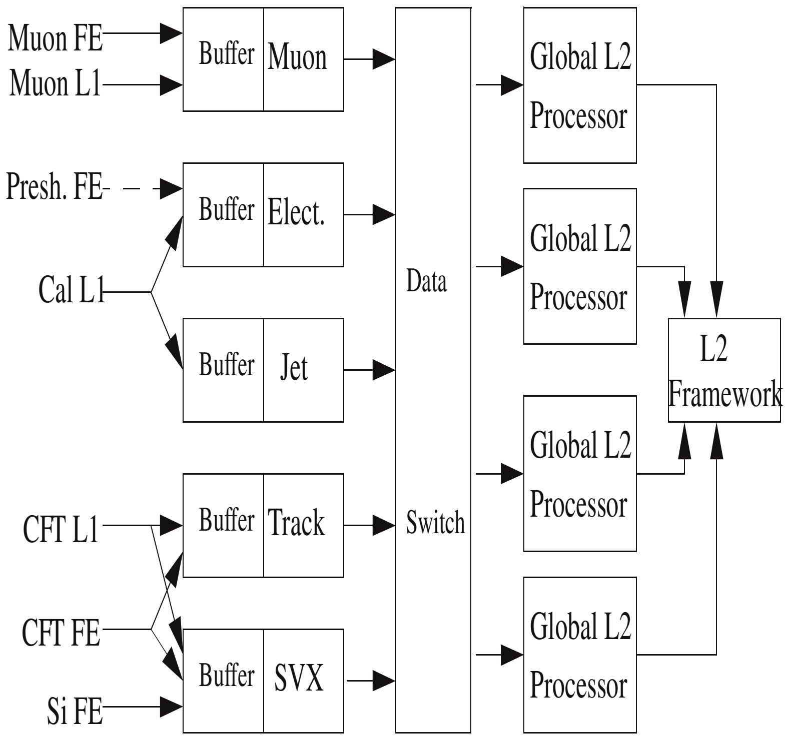

Figure 19: Overview of the L2 trigger components

latency and deadtime considerations as outlined below. Restricting the L2 trigger to use only concentrated data has a number of design advantages and allows the L2 trigger to focus, not on bulk data handling, but on its principal strength; the ability to make trigger decisions based on the correlation of information from a number of detectors.

In principle, at any given time all preprocessors are preparing information for the same event. When this process is completed, *i.e.* all preprocessors are done, all information pertaining to this event is transferred to a global processor. The amount of data transferred per event varies, but is of order one kbyte. The possible hardware/software solution used for this transport is generically referred to as a data switch for the purpose of this report. This switch can be realized in many different ways and the progress in this technology is very rapid. Although the choice of this data switching device is not completely determined, we base our current design on using an ATM switch here.

The global processor which receives one complete event is programmable and all processors contain identical versions of the trigger scripts. The scripts and/or the parameters that of the character of the signals available to the L2 system from L1 or the detector trigger outputs.

Since the last PAC submission, the understanding of the trigger system has been solidified with detailed timing simulations of the overall trigger system, which have led to the incorporation of L2 preprocessors which prepare lists of compacted information for transmission to the event processors. This feature is crucial in allowing affordable data transfer rates. We have adopted the design principle that generic choices for preprocessor and global processor hardware and software should be made to avoid expensive one-of-a-kind designs and fabrication. We also have designed the system so that the trigger system can be operated in a 'Mark and Pass' mode essential for trigger verification, and that the information used to arrive at an event pass or reject decision is available to the higher L3 system.

In the following sections we describe the current design in some detail, present some results of our simulations. Sufficient work has been done to understand that cost-effective solutions are available, and that the required trigger rejection for operation at $\mathcal{L} = 2 \times 10^{32}\mathrm{cm}^{-2}\mathrm{s}^{-1}$ can be obtained. The basic architecture of the system and the time frame in which the elements must operate has been established. Specific realizations of the L2 trigger have been examined to the extent that a costing of the system can be made, but we expect that as work continues many details will be modified, and more cost-effective and powerful solutions will be found.

4.2 Proposal for the L2 Trigger

Many different arrangements can be thought of for the various components in the L2 trigger and we have considered several of them. The case of a processor farm has been studied in some detail and based on those studies we have arrived at the current design. This system will consist of a set of preprocessors, which are detector specific and prepare the information to be sent to a farm of global processors. The global processors each work on one event at a time and are connected to the preprocessors through a data switching device. An overview of this system is shown in Fig. 19. In the following we describe the system in more detail.

The principal choice made in the L2 trigger design was to not work directly with the raw detector data but rather with "concentrated" information from the detectors. This choice is dictated by the very limited time available for the L2 system to reach a decision. The concentrated information is available from either the L1 trigger system for a detector or else from the detector front-end (FE) through a special preprocessor. As shown in Fig.19, each major detector system: muon, calorimeter, tracking (CFT), preshower and silicon vertex (Si) feeds data into a specific preprocessor. The result of each preprocessor is a list of candidate objects from that specific detector: muons, electrons, jets, tracks and secondary vertices. The number of preprocessors is limited and is determined by the number of detector systems. The calorimeter is a special case because its data are fed to two preprocessors: one for jets and one for electrons. The electron preprocessor also receives information from the preshower detectors.

The preprocessors will operate only on detector data from events that passed the L1 Trigger. They have a time budget up to about 75 μsec to prepare and deliver their data to the global processor farm of the L2 trigger (more details can be found in the timing section). This requirement is dictated by the 10kHz accept rate of the L1 trigger and simulations of

4 L2 Trigger for the upgraded DØ detector

4.1 Introduction

The DØ upgrade trigger system builds on the existing system in place for Run I, and was described in our April 17, 1995 submission to the PAC. The existing Run I trigger proceeds by a multi-stage set of decisions. Level 0 is an inclusive interaction trigger based on scintillator hodoscopes in the forward directions. Level 1 is a deadtimeless trigger based on calorimeter and muon PDT inputs operating in about 3 μs. Increased power is provided by the so-called Level 1.5 trigger system, based on processors operating in the 100 μs time frame, which refines muon information and allows more flexible construction of electron and jet objects. The final stage of triggering is done in the L2 board-level processors in which a fully assembled event can be analyzed with variants of offline algorithms.

The upgrade trigger system proposed originally in outline in 1990, and approved by the Laboratory in 1991, extends the power of these systems to meet the increased event rates and shorter bunch crossing times – and rationalizes the naming convention, with the old Level 1.5 becoming Level 2 (L2), and the old Level 2 becoming Level 3 (L3). The upgrade Level 1 (L1) systems described and approved previously operate in a few μs upon the trigger signals from single detector systems – calorimeter, fiber tracker/central preshower, forward preshower and muon chamber/pixel detectors. The L2 system described here makes decisions in a few hundred μs, typically combining data from several detectors to give refined information about physics objects present in the event. The L3 system remains a software trigger based on sophisticated algorithms operating on the full event.

The specifications for the input rates at each level of the upgrade trigger are: 10KHz out of L1: $\sim$ 1000 Hz out of L2, and $\sim$ 10 Hz out of L3. The deadtime introduced by the L2 system is less than 1%, while providing a factor of 10 rejection. The combined effect of the full trigger system is to reduce the raw inelastic collision rate by a factor of about 10^6 to select the interesting physics candidate events.

The L2 system described below obtains its rejection power by considering the correlations between trigger information from different detectors. We expect the specific correlation algorithms to evolve as experience is gained and new physics is added to the menu. The generic algorithms match spatial information in different detectors and compute correlations (mass, etc.) for multiple objects. Specific examples envisioned include: calorimeter – tracker matches; preshower – calorimeter matches, determination of jet parameters with reasonable jet cone definitions, determination of E/p, and rough mass calculations for dileptons, di-jets, lepton–jet, etc.. We require the L2 trigger to have a high degree of flexibility for implementing new algorithms that are necessary to address new physics. In Run I, this flexibility paid off in many instances – new triggers for rapidity gap events, for specific η-region muons and di-muons, and dijet triggers were all introduced rapidly and efficiently as the physics interests evolved.

Our understanding of the rejection power afforded by the cross-detector algorithms operating in L2 has been developed through simulations and experience with Run I data. These rejection factors have been presented in earlier submissions to the PAC (April 1995) and give good understanding that the overall bandwidth goals are achievable in the face of the high rates and multiple interaction environment. The simulations are based on our understanding

p_T Threshold GeV/c	CFT	CFT·APHI TOF	CFT·APIXEL·BPIXEL· CPIXEL TOF
One interaction event			
3.0	128 kHz	1.9 kHz	$<$ 0.3 kHz
10.	2.9 kHz	$<$ 0.3 kHz	$<$ 0.3 kHz
Six interaction event			
3.0	47 kHz	4.6 kHz	0.14 kHz
10.	36 kHz	2.8 kHz	0.039 kHz
Eight interaction event			
3.0	2.6 kHz	0.28 kHz	0.01 kHz
10.	2.3 kHz	0.18 kHz	0.0081 kHz

Table 6: Single muon one interaction rates in the central regionat a luminosity of $2 \cdot 10^{32}$ $cm^{-2}s^{-1}$ with 132 ns bunch spacing

p_T Threshold GeV/c	IROC A·B (cent)	A·B·C (cent)	A·B ·C (trigger)
One interaction event			
3.0	1.1 kHz	1.1 kHz	$<$ 0.3 kHz
6.	1.1 kHz	1.1 kHz	$<$ 0.3 kHz
10.	1.1 kHz	1.1 kHz	$<$ 0.3 kHz
Six interaction event			
3.0	0.21 kHz	0.14 kHz	$<$ .04 kHz
6.	0.21 kHz	0.14 kHz	$<$ .04 kHz
10.	0.21 kHz	0.14 kHz	$<$ .04 kHz

Table 7: Single muon one interaction rates in the forward region at a luminosity of $2 \cdot 10^{32}$ $cm^{-2}s^{-1}$ with 132 ns bunch spacing

mb cross section to each of the samples and then multiplying by the percentage of one, six, and eight interaction events assuming 132 ns bunch crossing.

One can see that the rates for single high p_T muons are within the 10 kHz Level 1 bandwidth. Note again that our trigger algorithms are still being optimized and further rejection is expected. Studies of low p_T dimuon rates are in progress.

The cost of the full Muon system and the associated Level 1 trigger is presently being finalized. The approximate M&S cost is about $1.1M for the Muon Level 1 trigger system, and $7.4M for the Muon detectors and the associated front-end electronics.

The Level 2 accept bandwidth is smaller. The maximum mean rate is 1 kHz for Level 2 accepts. If again a 10 Mbyte/s link is used, it is obvious that at 12 μs per event transfer time, a small fraction of the link bandwidth would be used. We can easily transmit data on the cables already installed. The use of all digital systems should also greatly simplify operation. The design for Run II allows a full test of every aspect of the system operation.

The trigger system will consist of three crates corresponding to the central region and each of the two end regions, and each of these regions is divided into octants that are handled by a pair of trigger cards. For each pair of cards, one makes decisions based on fast scintillator information and the other makes decisions based on wire information. The Level 1 muon trigger uses both types of information in a user-defined manner to determine whether a good Level 1 muon trigger has occurred.

3.6.2 Trigger Simulation

The muon trigger rates shown in Tables 6 and 7 are estimated using a software trigger simulator applied to one, six, and eight interaction two-jet events processed with GEANT. The simulation contains the geometries for the central barrel scintillation counters (APHI), cosmic ray scintillation counters (CS), three layers of pixel scintillation counters (APIXEL, BPIXEL, and CPIXEL), and three layers of Iarocci tubes (IROC) with four, three, and three planes in the A, B, and C layers. Shielding in both the forward and EC endcap regions is also present in the simulation. The central fiber tracker (CFT) geometry used has 8 layers.

In the central region, a single algorithm looks for coincidences between the APHI counters and CFT fine centroids. Time-of-flight cuts in the APHI counters are applied. Small efficiency losses between the octants are not included. Separate algorithms are used for plus and minus muon charges. Note that the rejection of the muon trigger in the CF region can be greatly increased by including the cosmic ray counters and/or centroid coincidences from the proportional drift tubes. This algorithm is still in progress.

In the end region two independent muon triggers were examined. One is based on the CFT tracker and PIXEL hit information. Time-of-flight cuts are applied to all three PIXEL layers. This algorithm first requires coincidences between the APIXEL counters and a corresponding range of CFT fine centroids. Separate algorithms are used for positive and negative muons. For each good APIXEL-CFT coincidence the algorithm further requires a good coincidence between the APIXEL, BPIXEL, and CPIXEL counters in R and phi coordinates.

A second algorithm in the end region, based only on the Iarocci tube (IROC) hits, was also evaluated. In this algorithm one first forms centroids (hit stubs) for each layer by combining hits from the planes in that layer. Centroids are formed by specific combinations of hits in three-out-of-four planes in the A layer and two-out-of-three planes in the B and C layers. Once centroids are formed, the trigger algorithm searches for good coincidences between centroids in the A, B, and C layers. In addition to the background rates found with this trigger, the rates requiring any A and B layer centroid and the rates requiring any A, B, and C layer centroid are shown in Tables 6 and 7.

All three algorithms were implemented in a trigger simulator. Using samples of single muons, the validity of the three algorithms was checked by plotting efficiency curves for each. Background rates were determined by running samples of one, six, and eight overlaid two-jet events through the simulator. The rates shown in the tables are obtained by assigning a 40 are 100% correlated, the method [10] gives us an Iarocci-based rejection of combinatoric background triggers of a factor of 100 ($\mathcal{L} = 2 \times 10^{32}$ cm^{-2} s^{-1}, 396 ns bunch crossing time). Taking into account the possible match between Iarocci-octants and pixel-towers, additional background rejection can be obtained. Our estimates show that the proposed detectors can be used for muon triggering and track reconstruction up to the $\mathcal{L} = 10^{33}$ cm^{-2} s^{-1} range.

Typical fluxes of electrons/positrons vs. distance from the beam axis are presented in Fig. 18. For $|\eta|$=2, the distance from the beam pipe is around 1.5 m. In this region the variation of background fluxes is relatively small. Using average fluxes from Fig. 18 and the method from Ref. [10], we can estimate the single muon trigger combinatoric rates for pixel counters. For $\mathcal{L} = 2 \times 10^{32}$ cm^{-2} s^{-1} and bunch spacing of 396 ns, the rate will be around $2{\times}10^2$ Hz ($1.0 < |\eta| < 2.0$). The accidental coincidence rate is proportional, in our case, to $\mathcal{L}^3$ while the real muon rate increases only linearly with luminosity. Any correlations between hits in the A, B and C-layers will increase background trigger rates. Extensive studies are needed in order to make more accurate background estimations. Direct measurements of correlations are being made using test pixel counters installed in the collision hall during Run Ic.

3.6.1 Trigger Electronics

The complete hit map for a particular collision cannot be determined until the maximum drift time has elapsed. Since the sensitive time of the detectors is greater than the crossing interval, the trigger logic cannot correlate hits and crossings. Thus the Level 1 trigger hardware will use the auxiliary fast detectors to eliminate most of the false candidates.

The need to have high rejection and low deadtime dictates the use of multiple levels of triggering. In order to eliminate deadtime, there must be a way of storing data long enough for a trigger decision to take place. For the TMC, this storage is already present in the chip. For the ADCs, we must supply a pipeline and tag bits externally. If the trigger latency is of order 4 μs, then the pipeline has to be about 100 locations deep. The Level 1 trigger must report a unique bunch crossing as the source of the interaction The fast detectors consist of the Cosmic Cap and the A-ϕ counters for CF, and the Pixel counters for the EF.

The trigger logic generates a new candidate list of hit bits at a 8 MHz rate (in the case of 132 ns crossings). The need to send trigger bits to the Level 1 processor at this speed defines the bandwidth requirements for the highest speed link in the muon system. One WAMUS chamber can generate a maximum of 96 hits. Six 16 bit words must then be sent every 132 ns which is 90 Mbytes/s. Relatively low cost serial links with rates as high as 1 Gbit/s developed for telecommunications have recently become available. These links meet the Level 1 bandwidth requirements and carry data on a single coaxial cable or optical fiber.

The Level 2 input bandwidth requirements will be much lower than the Level 1. In the worst case WAMUS chamber can produce 32 hits (30% occupancy). These hits could be encoded in about 120 bytes. If we assume a link bandwidth of 10 Mbyte/s, the event is transferred to the Level 2 processor in about 12 μs, a fraction of the 100 μs Level 1 accept time. Tests have been performed to determine the maximum bit rate sustainable on the coaxial cables presently used for sending analog data to the MCH from the platform. It appears that 160 Mbit/s rates can be transmitted over these lines, more than adequate for the Level 2 trigger requirements.

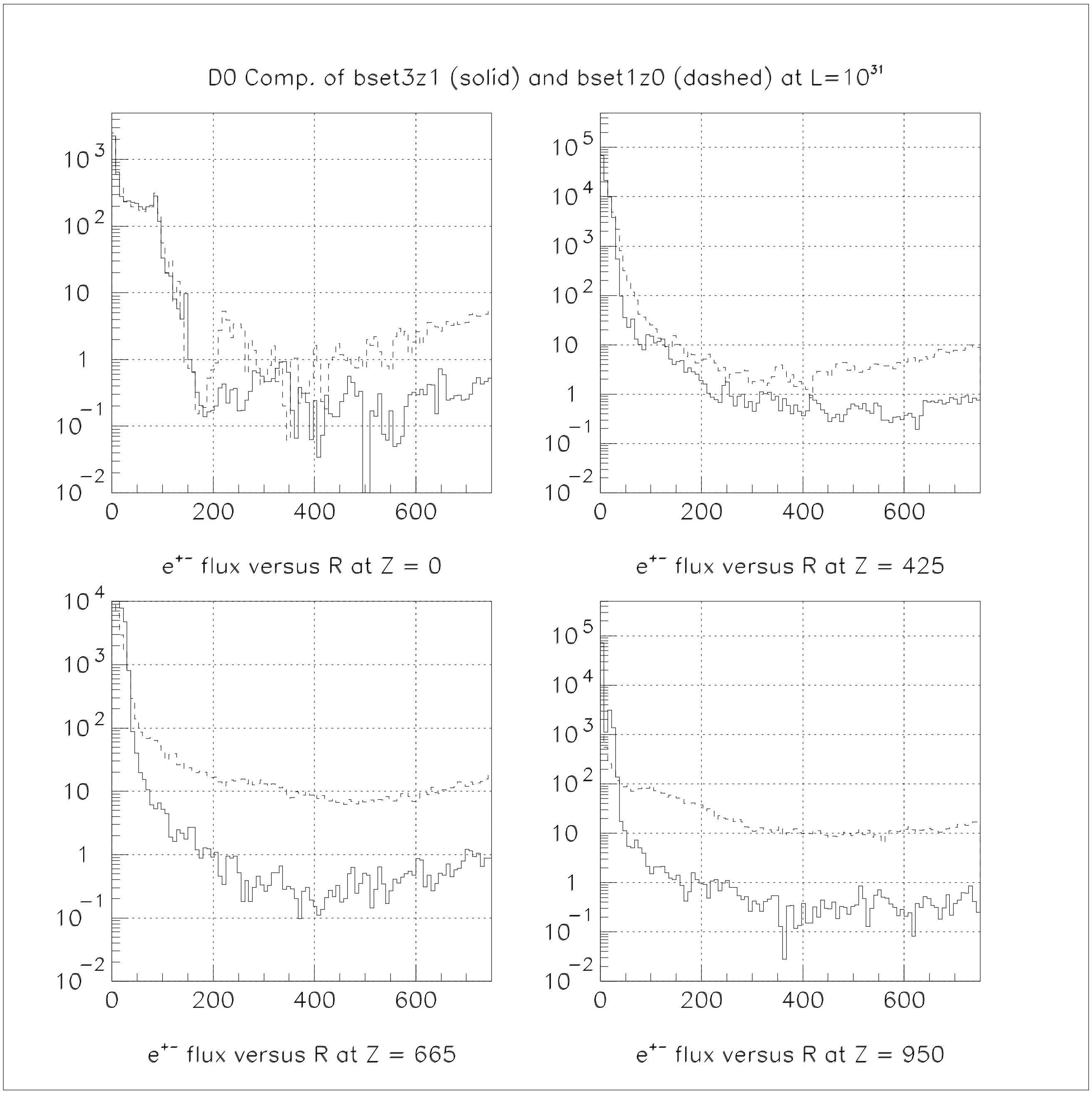

Figure 18: Radial (in cm) electron/positron flux distributions for different z positions: for unshielded (dotted) and shielded (solid) scenarios. The luminosity for this plot is $1 \cdot 10^{31}$ $\mathrm{cm}^{-2}\ \mathrm{s}^{-1}$.

The drift times themselves determine the muon momentum. On a test chamber using cosmic rays, we have achieved 0.4 mm resolution. For WAMUS, even with a fast gas (V_d^{-1} = 16 ns/mm), this implies a time resolution of 6.4 ns or a least count of 22 ns. Clearly, the time difference requirement drives the specification and the TMC resolution makes a small contribution to the drift distance measurement error. In the 48,000 channel Iarocci tube system, each input channel will have a latch similar to the scintillator counter card design and a digital delay based on commercial 18 bit FIFO instead of the TMC chip. This will allow deadtimeless operation for all the components of the muon system.

3.5.3 Charge Integration

At present, pad charges are sampled synchronously with the bunch crossings. The majority of the charge is delivered in 350-400 ns and we will sample only for this time. The new charge preamplifier will feature a reset switch to eliminate saturation problems, and reduced input impedance in order to collect the pad charge as rapidly as possible. The new pad integrator has about the same wide band RMS noise (1.2 mV) as the old amplilfierand the same gain (300 mV/pC). The recovery time of the integrator is about 20 ns which allows us to use a reset pulse 50 ns wide.

The pulse height ratio in the pads yields the coordinate orthogonal to the drift direction. For the pad repeat pattern of 61 cm, we achieved a resolution of $\sim$2 mm on a test chamber. In order to achieve that resolution we need to make 1% measurements of the individual pad pulse heights. This performance can be achieved with low cost 10 bit 15 Msps ADCs.

3.6 Trigger

There are two major components of the trigger rate at a given luminosity: real muon rates (π/K decays, heavy quark decays, W/Z, Drell-Yan, *etc.*) and background (combinatoric) rates. The single inclusive muon rates can be estimated with high precision using measured muon cross sections [33]. The typical single muon rate for $p_T > 3$ GeV/c is of order 1×10^2 Hz at $\mathcal{L} = 2\times10^{32}$ cm^{-2} s^{-1}. The real muon rate is reduced to a few Hz for p_T above a threshold of 10 GeV/c. The combinatoric background is considerably more difficult to estimate. The typical rejection needed in an inclusive muon trigger is 10^6 and therefore very large Monte Carlo samples are needed in order to make direct estimates. Rough estimates may be made by using a fully parametrized simulation based on expected detector occupancies [10, 11] or performing Monte Carlo calculations at high background levels (where trigger rejection is lower) and extrapolating to lower background levels [31].

The muon Level 1 trigger will include scintillation pixel counters, WAMUS PDT's or Iarocci tubes, and the central fiber tracker. The same devices, with finer segmentation, will be used at the Level 2 trigger. All DØ detector elements (including calorimetry for muon energy deposition confirmation and central tracking detectors) will be used for muon identification at Level 3.

Use of Iarocci tubes for the forward Level 1 trigger has two substantial advantages: the possibility of making a high p_T trigger (scintillator pixels can provide a p_T cut at 3 GeV/c or below) with a threshold around 10 GeV/c and additional reduction of combinatoric background. Even for the conservative assumption that the hits in planes of one layer plastic. This design has the advantage of a better photomultiplier connection and counter design, but fewer photoelectrons and a more complex assembly/production procedure. A time resolution of 0.8-1.4ns has been obtained for test counters. Both counter designs use 1 inch 115M photomultipliers from the Russian MELZ factory.

The total number of counters in the proposed system is 4,800. They are grouped into octants matching the Iarocci octants. There are about 96 counters per octant.

Calibration of the scintillation counters (time and amplitude) is necessary in order to maintain a high efficiency for muon detection. There are two options under consideration now: the use of a special calibration system (based on LEDs) or the use of muons with low p_T (around 3 GeV/c) produced at the interaction region. At $\mathcal{L} = 2 \times 10^{32}$ cm^{-2} s^{-1}, the inclusive muon rate will be of order 1×10^2 Hz. Estimates show that we can collect around 5×10^2 events per counter during a 30 minute calibration run. In order to select the appropriate calibration scheme, we plan to perform long term stability studies using prototype pixel counters.

3.5 Front-End Electronics

The front-end electronics for all the muon detectors will be replaced. The electronics design is well developed. The readout part of the WAMUS electronics is the basic model for the fast trigger-detector electronics design.

3.5.1 Wire Amplifier

The wire amplifier design takes advantage of new, lower power commercial IC's to achieve comparable noise performance to the present system. Performance improvements include the addition of transformer coupling at the service boards to provide a true differential connection and avoidance of low impedance ground paths between the chambers and the preamplifier inputs. The determination of which tube in a pair is hit will be achieved by separating the arrival time by about 20ns, through the use of a lumped constant delay lines in series with the jumper joining the far ends of the tube pair. Similar preamplifiers can be used for the Iarocci tube system.

3.5.2 Time Digitization

The drift time measurement will be made with a four channel pipelined digital TDC chip (TMC) developed by Arai at KEK[37], which matches our needs very closely. The bin width, when run at 26 MHz, is 1.2 ns and the maximum delay is 4.8 μs, enough to cover the Level 1 trigger latency of 4.1 μs. The pipeline can store one hit per clock cycle, which means that there is no limit to the maximum number of wire hits recorded during one drift time interval.

The time of arrival difference between each end of the WAMUS tube pairs is used to break the ambiguities of the repetitive pad pattern. For a least count time ΔT, the resolution is $\sim c \cdot \Delta T/5$. Therefore, to resolve the pads (L = 61 cm) with a resolution of 30 cm, a least count of $\sim$ 5 ns is required. We propose to calculate ΔT by subtracting time values from adjacent tubes.

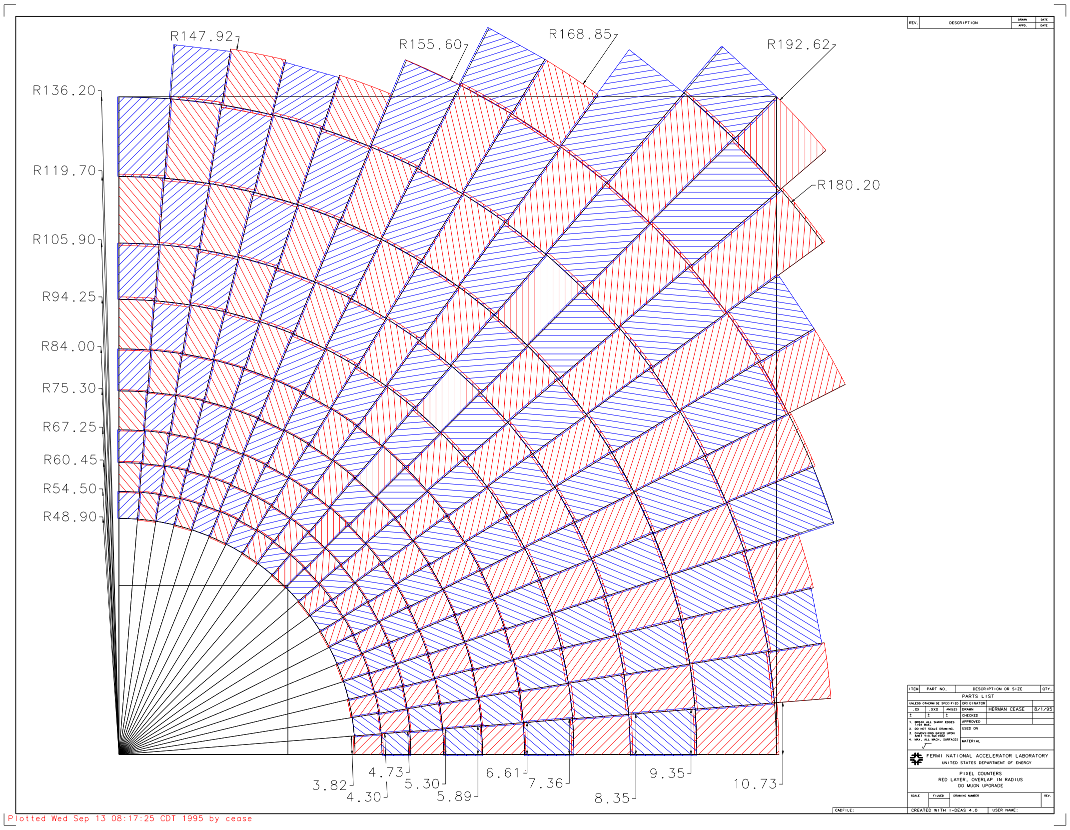

Figure 17: One quadrant of scintillation pixel plane.

3.4.2 Scintillator Pixel Counters

The time and energy spectra of background particles are substantially different than those from real muons. Scintillation counters will register substantially fewer background hits than other types of detectors [31, 23]. Use of a 20 ns gate (instead of 100 ns) reduces the number of background hits per plane by a factor of five. The minimum ionizing energy deposition in 1/2 inch plastic is 2.5 MeV. Setting a detection threshold at 0.5 MeV will reduce the counting rate due to neutrons by a factor of three[32].

We propose to install three layers of scintillation counters (A, B and C-layers) with $\Delta\phi = 4.5^\circ$ and $\Delta\eta = 0.1$ segmentation in the forward region (Fig. 17). This segmentation has been optimized with respect to multiple scattering, the fiber tracker trigger azimuthal segmentation, the minimum muon momentum, background trigger rates, and the number of channels [10]. Each plane consists of two overlapped sub-planes in order to remove any dead zones between counters. The maximum counter size is 60×110 cm^2.

There are two options for the pixel counter light collection design under detailed study. The first is based on two WLS bars used for collection of light into the photomultiplier [31]. The high transparency of Bicron BC404A 1/2" scintillator provides a large number of photoelectrons (more than 60 for the largest counters) and good uniformity (within $\pm10\%$). In the second design, twelve 1 mm diameter WLS fibers (Bicron G2 fibers with decay time of 2.7ns) are installed over the counter perimeter to collect light from all four sides of the

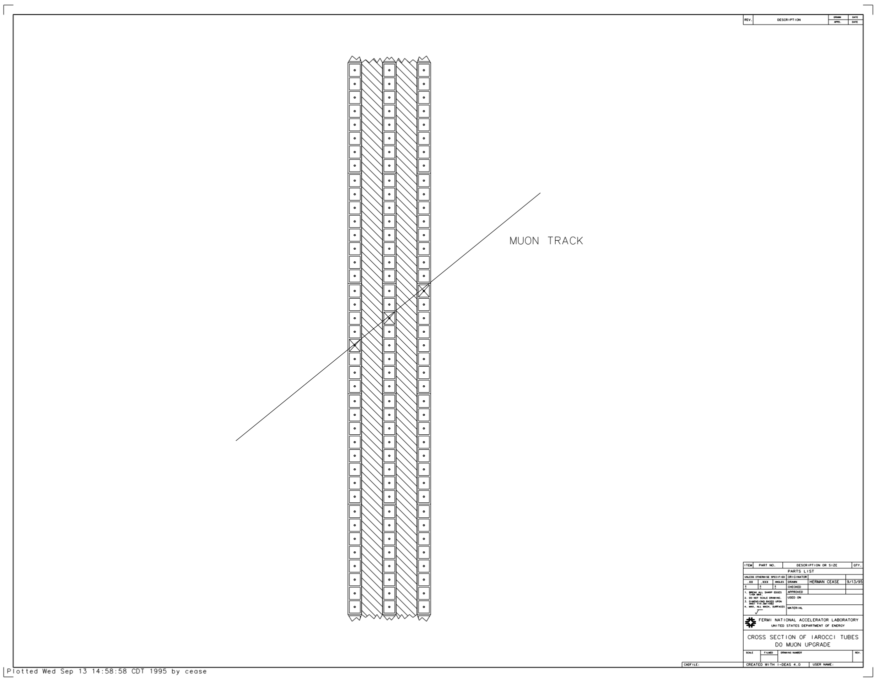

Figure 16: Iarocci B and C-layers design

muon system is limited by multiple scattering and the coordinate resolution of the muon detector. The typical coordinate resolution of WAMUS and SAMUS detectors (per layer) in Run I was around 1 mm. Mechanical inaccuracies, survey accuracy, and the time-to-distance calibration are the major factors limiting resolution. For three planes of Iarocci tubes, the per layer effective coordinate resolution is around 1.4 mm.

The total number of Iarocci 8-tube modules is 6,000 (48,000 individual channels). They will be produced and tested at JINR (Dubna) and shipped to FNAL for final assembly. We plan to use the existing SAMUS high voltage (HV) and gas systems. These HV power supplies can produce currents sufficient for operation at the Run II design luminosities. In total, 48 HV channels will be used: one per octant.

We plan to use Iarocci tubes for both track reconstruction and triggering. Since the gate width can be set below the 132 ns bunch crossing time, simple amplifiers/latches can be used. $R-\phi$ cathode pads on the surface of Iarocci planes could be used for additional background trigger rejection, but are not part of our proposal.

Experience with SAMUS tubes shows that an integrated charge of 50 C/cm on the anode wire can be accumulated without changes in gas amplification using a freon-methane gas mixture (similar to the one we propose for the Iarocci tubes). Preliminary studies of the Iarocci tubes show that there is no outgassing from their internal surfaces. This suggests that Iarocci tubes can run for many years at $\mathcal{L} = 1 \times 10^{33}$ cm^{-2} s^{-1} without aging. Studies of Iarocci tube aging with the selected gas mixture in the proportional mode are underway.

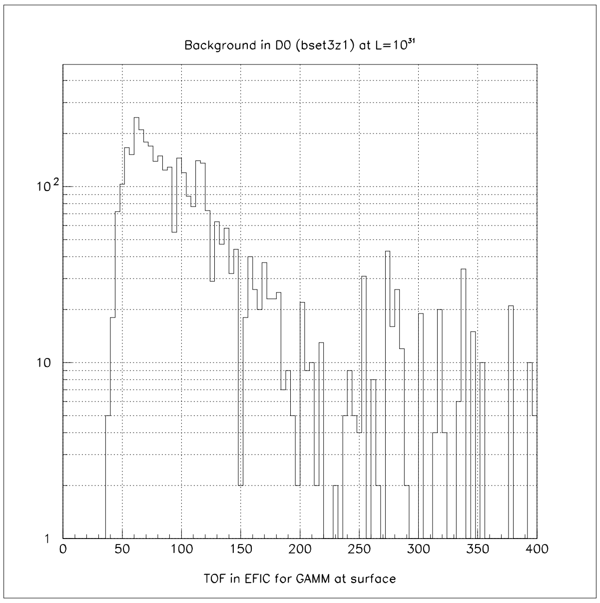

Figure 15: Time distribution [ns] of hits in C-layer of muon detectors. The real muon peak is at 27 ± 7 ns.

There is a long time tail with decay time around 2 μs. Overlap of these tails from many crossings provides an almost uniform background.

An additional advantage of Iarocci drift tubes is the small gas volume. They have five times lower sensitivity to fast neutrons than the WAMUS chambers [30].

The intrinsic efficiency of an individual Iarocci tube is near 100%, but due to the tube walls, the efficiency of a plane is 90% (1 mm wall/10 mm cell). In order to have a track vector from each layer the planes will be separated by 10-20 mm (see Fig. 16). In order to reduce the probability of track segment formation by low energy electrons, the gap between the Iarocci planes will be filled with polyethylene plates. The energy of electrons from neutron interactions is below 1 MeV and they can be absorbed by 5 mm of polyethylene.

To reconstruct muon track segments, at least two hits per layer are needed. For three planes per layer (as shown in Fig. 16) the efficiency for two-out-of-three hits is 97%. For the B and C layers we propose to use three planes of Iarocci tubes per layer, while the A-layer has four planes since the A-layer background flux is a factor of 3 higher than for B and C. In order to detect soft muons (that range out in the EF toroid) we will use three points on an A-layer track segment: two to find a segment and the third to confirm it (any two hits will provide a “segment”). The 3-out-of-4 efficiency is above 91%. The reasonably large number of points on a track will improve the accuracy of the track reconstruction (both the momentum resolution and the match with the central detector) and make track reconstruction algorithms more robust. The 4(A-layer)+3(B-layer)+3(C-layer) design is similar to the central WAMUS design.

The solenoid tracker momentum resolution falls off in the forward direction and the contribution from the muon system becomes significant. The momentum resolution of the

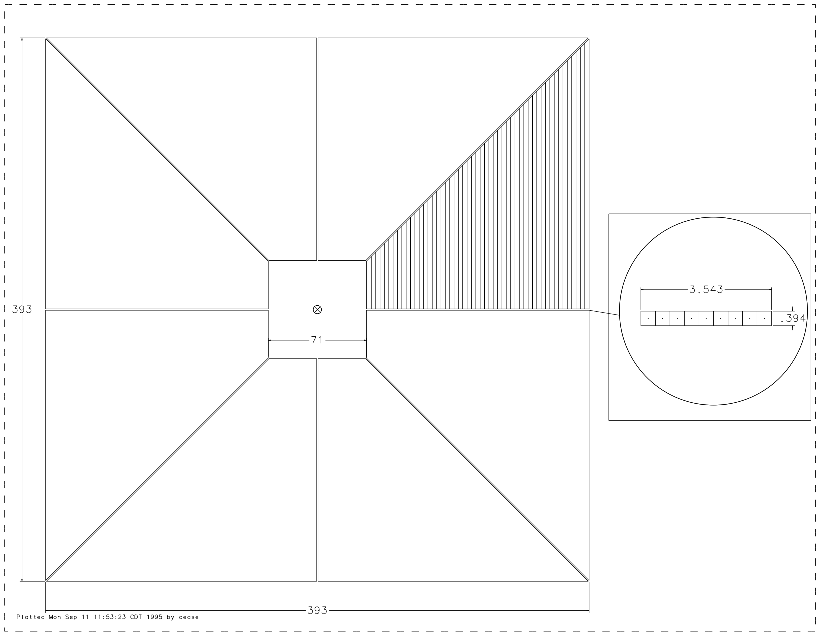

Figure 14: Iarocci proportional tubes: individual 8 tube module and one complete plane

with a TDC. The latched hits will be used in the Level 1 trigger. An electronics pulser and an LED light pulser will be used for time and gain calibration.

3.4 Forward Muon Detectors

Iarocci tube planes and scintillation pixel counters are proposed for the forward muon triggering and track reconstruction.

3.4.1 Iarocci Tube System

The Iarocci tube design has a 10×10 mm^2 internal cross section with 50 μm anode wires in the center of each cell. The tubes, in packs of eight, are made from plastic extrusions as long as 5 m. The internal surfaces of the tubes are covered with conductive paint (1 kΩ/square) to form the cathode electrode. This type of detector has been used extensively in collider experiments [29]. Filled with a fast gas mixture (such as Ar(80%)+CF_4(10%)+CH_4(10%), these tubes will have a maximum electron drift time of 60 ns. The planned gate width of 100 ns is well within the 132 ns bunch spacing.

The layout of one Iarocci plane is shown in Fig. 14. The tubes are oriented along magnetic field lines (the field shape in the EF toroids is more "square" than "circular"). The flux of particles decreases with increasing distance from the beam pipe. Using the geometry shown in Fig. 14 the occupancy of individual tubes will vary only a factor of two over the entire plane.

A typical time distribution of C-layer hits is shown in Fig. 15 (with shielding discussed above). This figure was obtained from a GEANT simluation for a single bunch crossing.

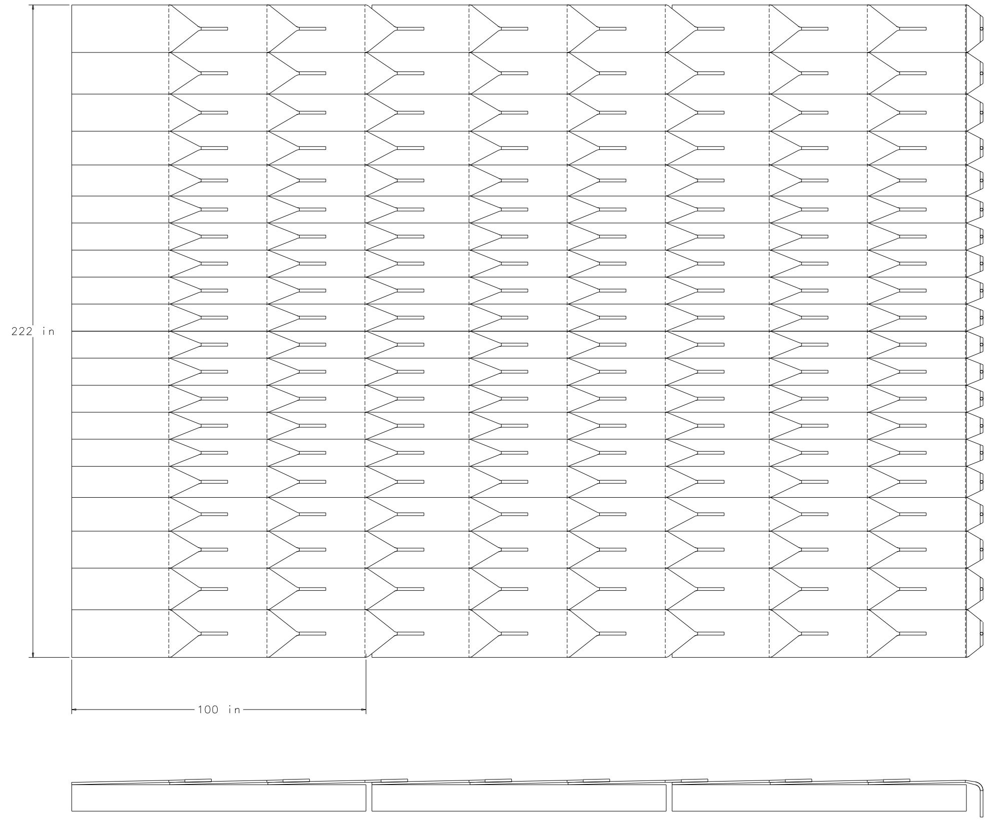

Figure 13: The A-ϕ counter array of the east or west wall A-layer.

The CF C-layer bottom is located underneath the North and South ends of the platform and consists of approximately 40 counters with a design similar to those described above.

3.3.3 A-ϕ Scintillation Counters

The "A-ϕ" scintillation counters [23] will be located between the Central Calorimeter and the WAMUS central A-layer PDTs. The purpose is to provide a ϕ measurement matching high and low p_T triggers with the central tracking chamber to reject out-of-time backgrounds originating at or near the exit of the calorimeter. The counters divide the A-layer into rows covering $\sim 4\frac{1}{2}$ degrees of ϕ. Each row contains nine counters that cover three 100 inch wide PDTs. Because the geometry is box-like, the counter widths vary from 10 to 17 inches. Figure 13 shows a view of the A-ϕ scintillator array on the east or west A-layer wall. The scintillator is $\frac{1}{2}$ inch thick Bicron 404a and light collection is accomplished with Bicron G2 waveshifter fiber. This waveshifter has a fast (2.5 ns) decay time and is well-matched to the scintillator and PMTs. The photomultipliers are Russian MELZ 115M tubes which have a 1" diameter.

We have been operating test counters in the CF A-layer during this collider run and have verified that muons are well separated from the background and in good agreement with Monte Carlo.[23]

All these counters will be outfitted with new, pipelined electronics for a deadtimeless readout. A hit "in-time" with a short gate will be latched and the time will be measured momentum resolution in the central region in Run II will be dominated by the central tracking system. The drift chambers produce the following measurements for each hit: the drift-time T perpendicular to the anode wire; the difference, ΔT, in the arrival time of the hit between a hit cell and its neighbor (jumpered at the far end), providing the distance along the wire; and the charge deposition on inner and outer vernier pads, yielding a more accurate measure of the distance along the wire. The Run Ib gas mixture is composed of 90% Argon, 6% CF_4 and 4% CO_2. The maximum drift time is 750 ns for a 5 cm drift, with the wires operating at 4.56 kV and the pads operating at 2.3 kV. In order to reduce the number of crossings which occur during one drift interval, we are considering using a faster gas mixture during Run II. The gain, drift-time-to-distance and aging characteristics of 80% Argon, 10% CF_4 and 10% CH_4 are being studied. Preliminary results indicate the maximum drift time can be reduced to 450 ns with the wires operating at $\sim$ 5.0kV and the pads operating at $\sim$ 2.5kV. The contribution to the hit uncertainty due to diffusion is estimated at less than 500 microns, worse than the present 300 microns, but smaller than the 700 micron residual typically achieved in WAMUS chambers during Run I. The trade-off in resolution is offset by the reduced occupancy and benefits to triggering achieved by decreasing the number of crossings in one drift time from 6 to 4 for 132 ns bunch spacing operation.

The electronics will be modified to provide a deadtimeless front-end readout with either 396 or 132 ns bunch spacing. We plan to read out the T and ΔT from all of the chambers. Although not instrumented initially in all chambers, hooks are built in to allow readout of the pad information. The latched hit cells will be available for the Level 1 muon trigger.

3.3.2 Cosmic Cap and Cosmic Bottom Counters

The Cosmic Cap counters [21] cover the top and sides of the central region with 12 divisions in ϕ and 20 divisions in z. The purpose is to provide a fast trigger detector outside of the toroid magnet and to tag the crossing for hits in the WAMUS CF B and C-layers. The background rate is small in comparison with other detector regions; very tight timing is not necessary to achieve adequate rejection. These counters exist and have been used during Run I. They have achieved timing resolution of 2.5 ns after offline corrections (online, the counters have timing resolution of $\gtrsim$ 5 ns).

The bottom of the central region was not covered with scintillation counters during Run I and must be done for Run II. The "Cosmic Bottom" includes the CF Bottom B- and C-layer counters and the EF Bottom B-layer counters. The design is similar to the Cosmic Cap: scintillator sheets with waveshifter fibers for the light collection. Forty counters will be located on the B-layer chambers underneath the muon toroid. These are referred to as the "CF B-layer Bottom" counters. A minor difference between these counters and the Cosmic Cap is that these counters will be oriented with the short dimension along ϕ so that they cover a slice approximately $4\frac{1}{2}$ degrees wide. The smaller ϕ segmentation is advantageous for matching with the CFT trigger tracks. The counters come in two sizes: $15\frac{3}{4}$ inches wide or $22\frac{3}{8}$ inches wide and $98\frac{1}{8}$ inches long. The narrower counters are located directly under the calorimeter supports where there is no A-layer coverage. A full-size prototype has been constructed and tested. Construction of these counters will begin in Tata Institute in February, 1996. The EF B-layer bottom, located on the PDTs just underneath the North and South EF toroid magnets, consists of 36 counters $\sim$ 88 inches long and $\sim$ $15\frac{3}{4}$ inches wide.

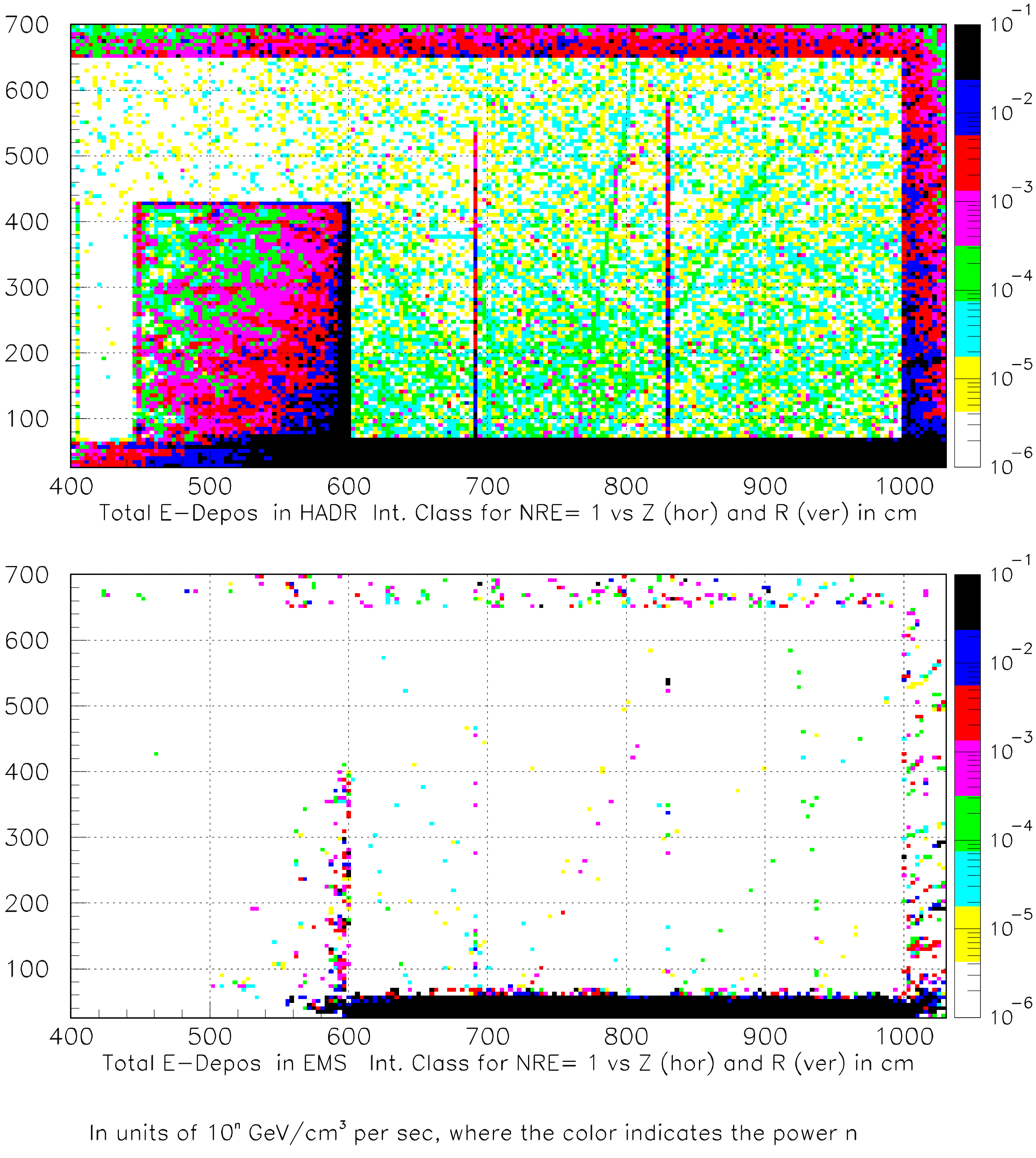

Figure 12: Energy deposition from hadrons (upper) and electromagnetic showers (lower) in the shielded detector. A luminosity of $2 \cdot 10^{32}$ cm^{-2}s^{-1} is assumed.

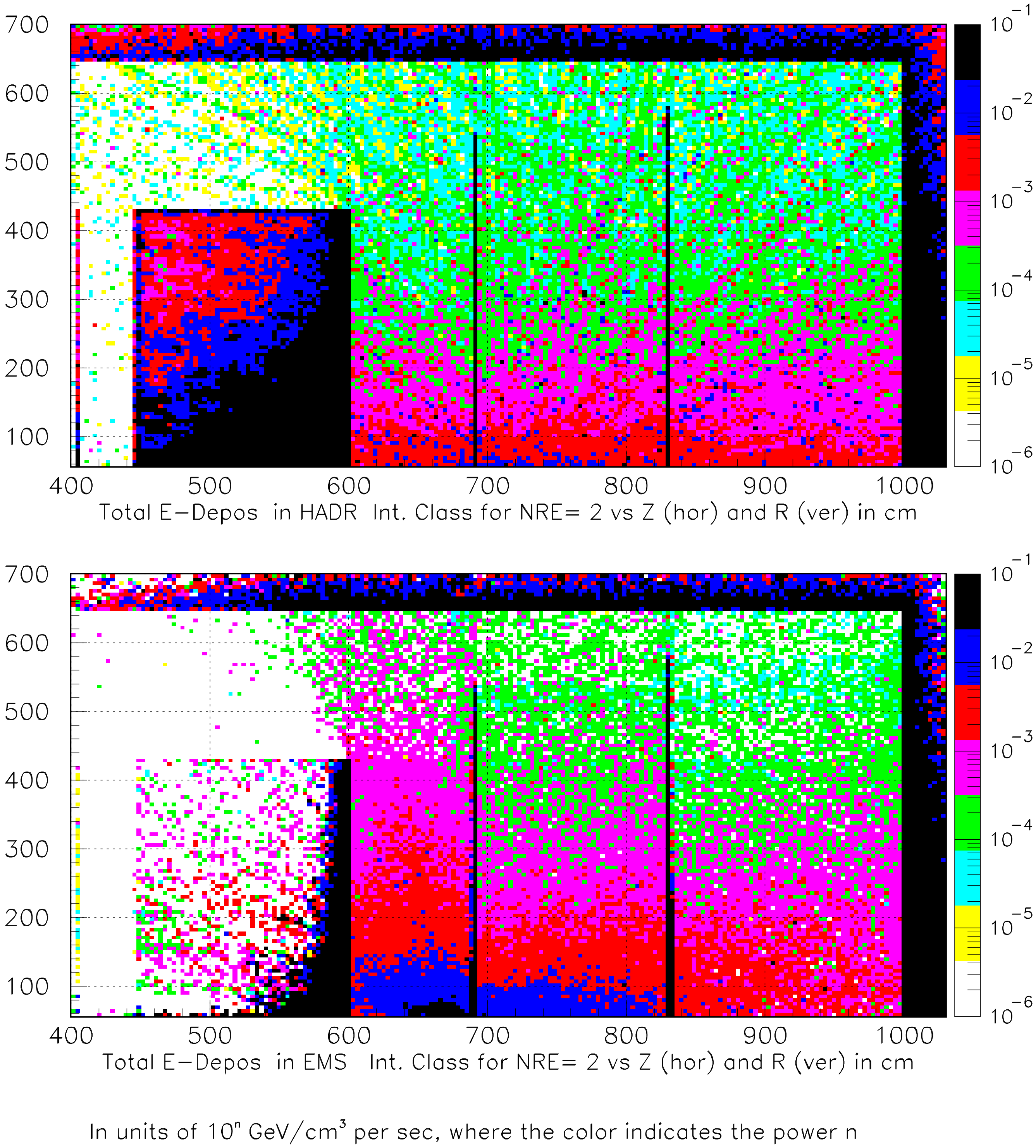

Figure 11: Energy deposition from hadrons (upper) and electromagnetic showers (lower) in the unshielded detector. A luminosity of $2 \cdot 10^{32}$ cm^{-2}s^{-1} is assumed.

Item	Layer		
	A	B	C
WAMUS PDTs (Drift Cells)	18 (1728)	38 (2424)	38 (2616)
Cosmic Cap Counters (PMTs)	-	-	240 (480)
CF Bottom B Counters (PMTS)	-	40 (80)	-
CF Bottom C Counters (PMTS)	-	-	40 (80)
EF Bottom B Counters (PMTS)	-	36 (72)	-
A-ϕ Counters (PMTS)	630 (630)	-	-

Table 5: Channel count for the various central muon upgrade detectors. These are sorted by layer, not including spare counters or electronics.

energy deposition from hadrons and electromagnetic showers in the Run I detector configuration for a luminosity of $2 \cdot 10^{32}$ cm^{-2}s^{-1}. Figure 12 depicts the energy deposition from hadrons and electromagnetic showers in the shielded detector. The effect of the shielding is striking.

We find that the energy deposition from proton and antiproton remnants is reduced by approximately a factor of 100 with a shield comprised of 39 cm of iron, 15 cm of polyethylene, 2 cm of lead and an additional 3.2 inches of iron located on the inner core of the shield at the exit of the muon toroid in front of the low-beta quadrupole magnet.

Additional polyethylene shielding will be mounted in the gap between the End Calorimeters and the EF toroids to reduce the rates in the CF A-layer detectors due to shower propagation at the rear of the calorimeters through the liquid argon and insulating vacuum space. These shields are shown in Fig. 10 as cross-hatched triangular sections.

3.3 Central Muon Detectors

The DØ muon detector is composed of detector planes arranged as the surfaces of a box, with the top, bottom, and sides forming the central region and the box ends the forward region. The boundary between the two regions is at approximately $|\eta| = 1.0$. While muon detection for the forward region is being completely redesigned for Run II, we will retain much of the present system in the central region. The 94 CF WAMUS drift chambers and the 480 scintillation counters of the C-layer "Cosmic Cap" will receive new electronics. New scintillation counters will be added to the bottom B- and C-layers and to the CF A-layer. They are shown in Fig. 10 and a channel count is provided in Table 5. The new detectors exploit features of the existing detector (thick calorimeter and iron magnet, small π/K decay volume, etc.), and add high rate capability and good time resolution.

3.3.1 WAMUS

The WAMUS central region consists of three layers of drift chambers, one layer inside and two layers outside the iron toroid magnet. The purpose is to provide muon identification and a confirming momentum measurement independent of the central tracking. (The muon

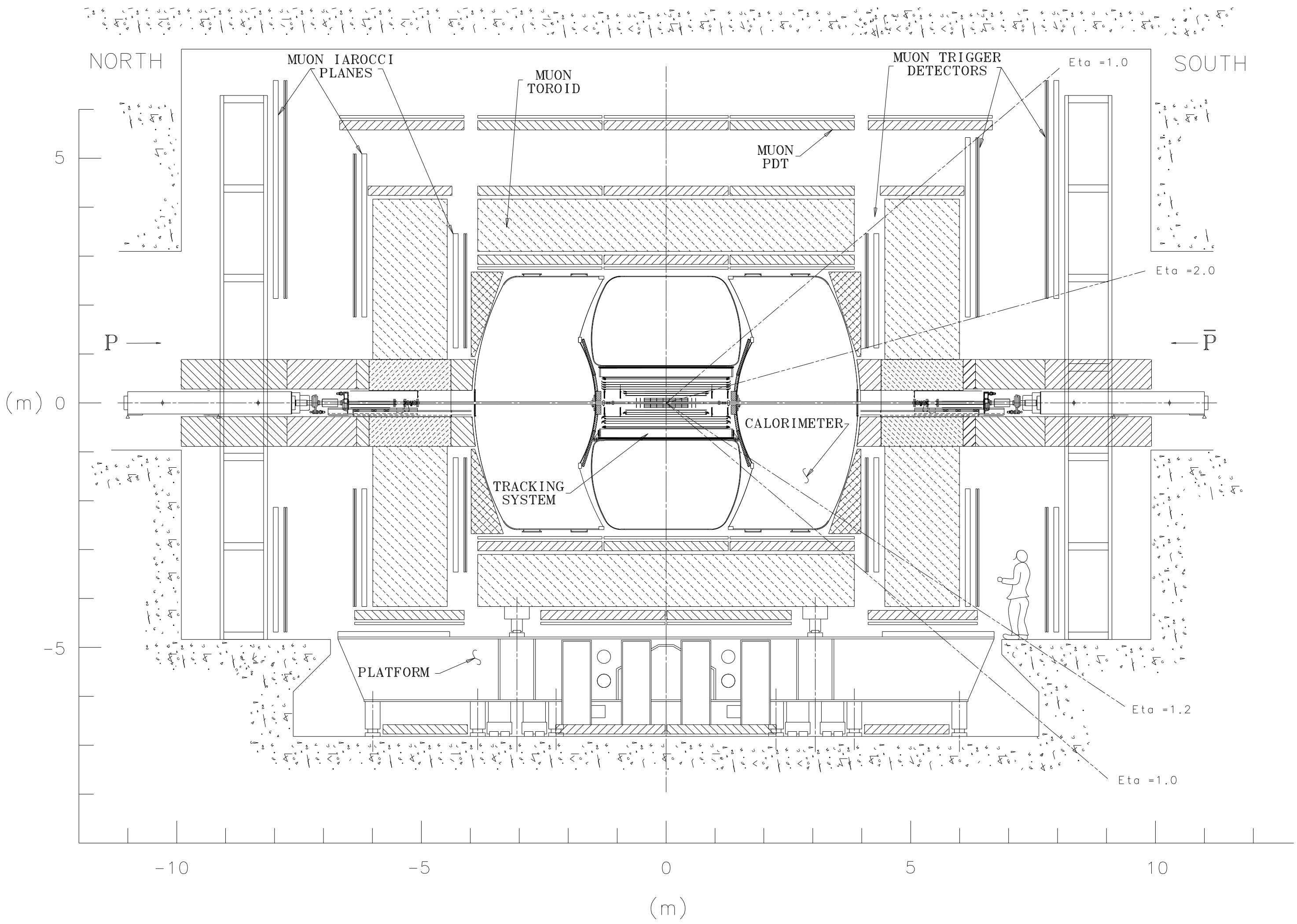

Figure 10: Side view of the DØ upgrade detector including the various elements of the muon system upgrade and the large scale shielding being considered.

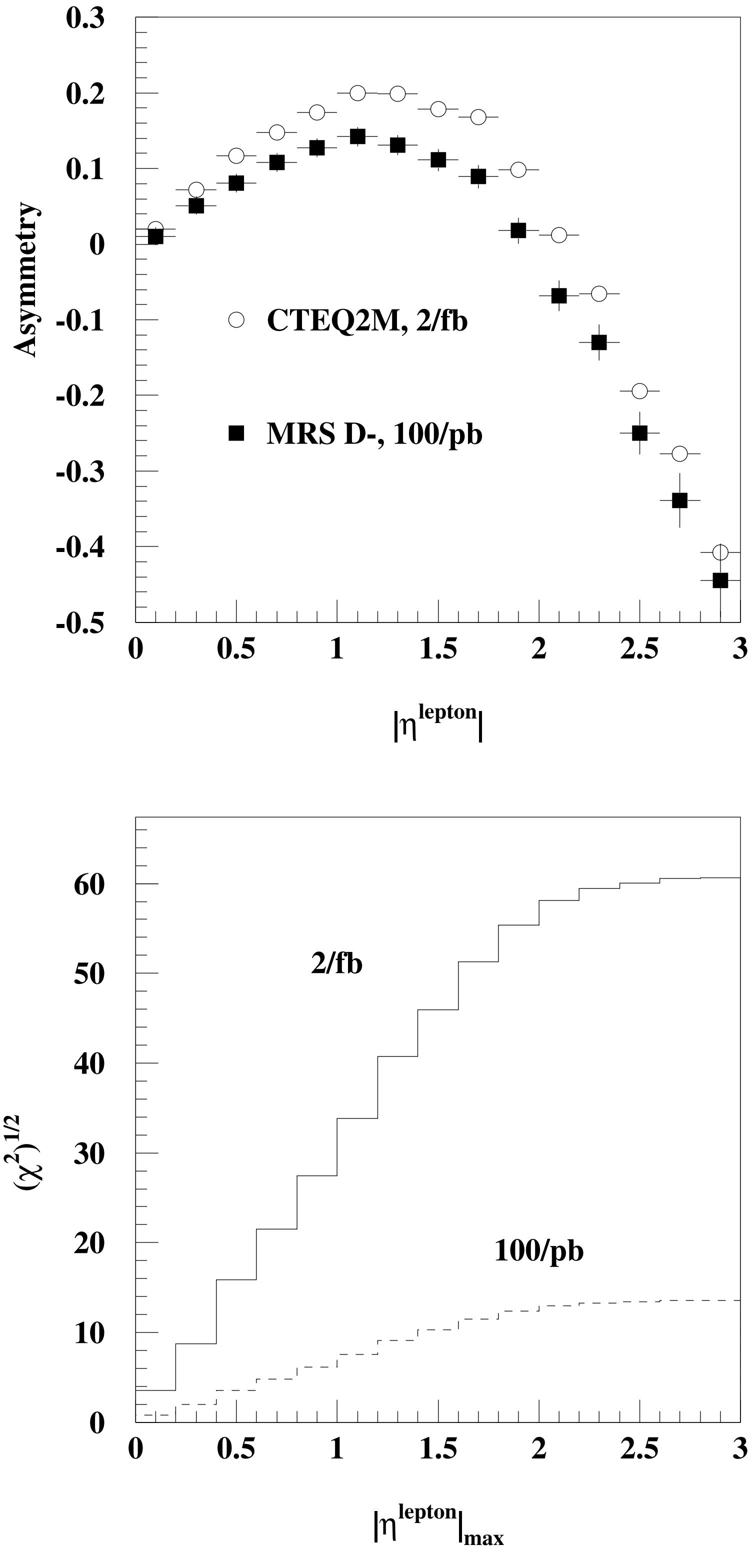

Figure 9: (Upper) The predicted lepton charge asymmetry for W decays is shown as a function of the lepton $|\eta|$. (Lower) The significance of the difference in the results from the CTEQ2M and MRSD- pdf's is plotted versus $|\eta|$ coverage.

The individual components of the new design will be discussed in more detail in subsequent sections; a brief overview is given here. In general, we have attempted to minimize the number of regional boundaries, chamber technologies, and distinct electronics boards. We have also built in hooks to allow a natural upgrade to $\mathcal{L} = 10^{33}$ cm^{-2} s^{-1}.

The three layers of the muon system are designated A,B,C, where A is closest to the interaction region, and the toroid magnet is located between the A and B layers. For $|\eta| \lesssim 1$, the WAMUS PDTs will be retained but the electronics, from the front-ends to the Movable Counting House (MCH), will be replaced. There will be two layers of scintillator: the current "Cosmic Cap" just outside the C-layer and a new set of "A-ϕ" scintillation counters located between the calorimeter and the A-layer, as discussed and approved over the past two years. There will be a CFT·A-ϕ trigger with good geometric acceptance that will enable a trigger on low-p_T muons ($\gtrsim 1.5$ GeV/c) in the central region. There will also be a trigger based on the hits in the PDTs, as in Run I.

For $1 < |\eta| < 2$, the PDTs will be replaced with planes of Iarocci-tubes. The tubes are square in cross section and 1 cm wide. They will be arranged in three planes (A,B,C) with (4,3,3) layers of tubes per plane. There will be three planes (A,B,C) of scintillator pixels arranged in an $R-\phi$ geometry. The trigger will be provided by a CFT·Pixel coincidence. As in the central region, a Run I-style trigger based on the Iarocci wires will also be implemented.

To summarize, we have converged on a new baseline design for the DØ muon system upgrade. The performance of this system will allow us to meet the challenges of Run II. However, we will need new tracking detectors for the forward region, in addition to the approved triggering planes, and, in order to provide enough shielding, we must restrict the forward coverage to $|\eta| \lesssim 2$. Therefore the Small Angle Muon System(SAMUS) stations will be removed after Run I. The upgrade system will survive the harsh environment of Run II and hooks are available to handle luminosities up to 10^{33} cm^{-2} s^{-1}. We are ready to complete the detailed design work and proceed to build the system.

3.2 Shielding

The upgrade of the DØ muon system will include the addition of shielding material. This shielding will block non-muon background particles originating from the three hottest sources [12]. The main source is scattered proton and antiproton fragments which interact with both the exit of the calorimeter (producing a background in the central and forward muon A-layer) and the beampipe and low-beta quadrupoles (producing showers in the forward B and C-layers). (The accelerator-produced background which comes from the tunnel is small compared to the direct contribution from interactions due to improved shielding that was installed in the tunnel during Run Ib [13].) Shielding these background sources is important because it will reduce the occupancy of the detectors. This decreases the fake trigger and track probabilities and increases the detector lifetime by reducing aging.

The main feature of the B and C-layer shield is a thick iron and polyethylene case surrounding the beampipe and final low-beta quadrupole magnet. This is shown in Fig. 10, extending from the calorimeter to the accelerator tunnel. The shield is ~ 67 inches wide on the outside and has an inside hole ~ 20 to 25 inches wide for the accelerator equipment.

The appropriate thickness of the iron and polyethylene was determined by Monte Carlo simulations (`GEANT` and `MARS`) for various shielding configurations. Figure 11 shows the

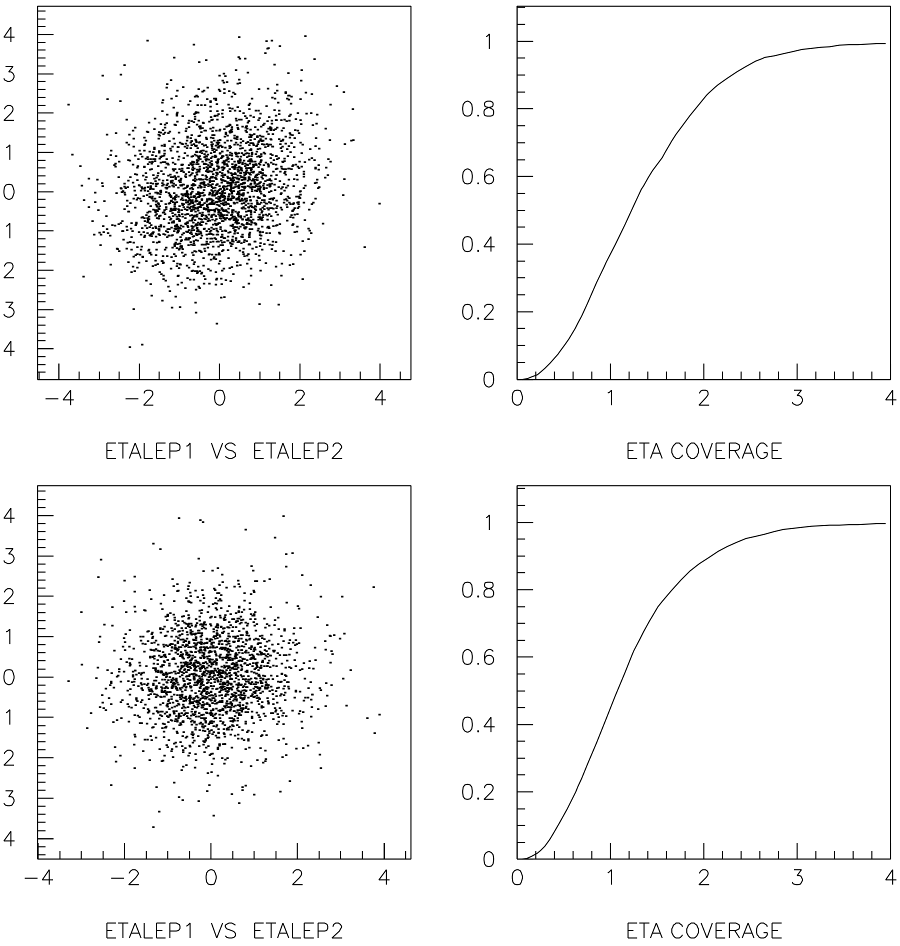

Figure 8: Shown (left upper and lower) are the $|\eta|$ distributions of muons from the decay of W's in WW production (upper) and $t\bar{t}$ ($M_{top} = 180$ GeV/c^2)(lower). The efficiency as a function of $|\eta|$ coverage of the muon detector is shown (right).

defined by the end of the CFT trigger, *i.e.* at $|\eta| \sim 1.7$. Studies of Run II trigger rates [10, 11] show that the combined muon/CFT trigger will be unprescaled for high-p_T single muons ($p_T > 8$ GeV) and low-p_T dimuons ($p_T > 3$ GeV). With the proposed shielding, the combinatoric trigger rate is dramatically reduced to the point where the trigger rate is dominated by real muons.

Triggering in the high rate environment of Run II requires the use of fast trigger elements with good time resolution. In the central region, the maximum drift time in the existing PDTs of 750 ns exceeds the Run II bunch spacing of 396 or 132 ns, and scintillators will provide the necessary time stamp. In the forward region, accidental triggers from uncorrelated particles in the three layers will be reduced by scintillator pixels.

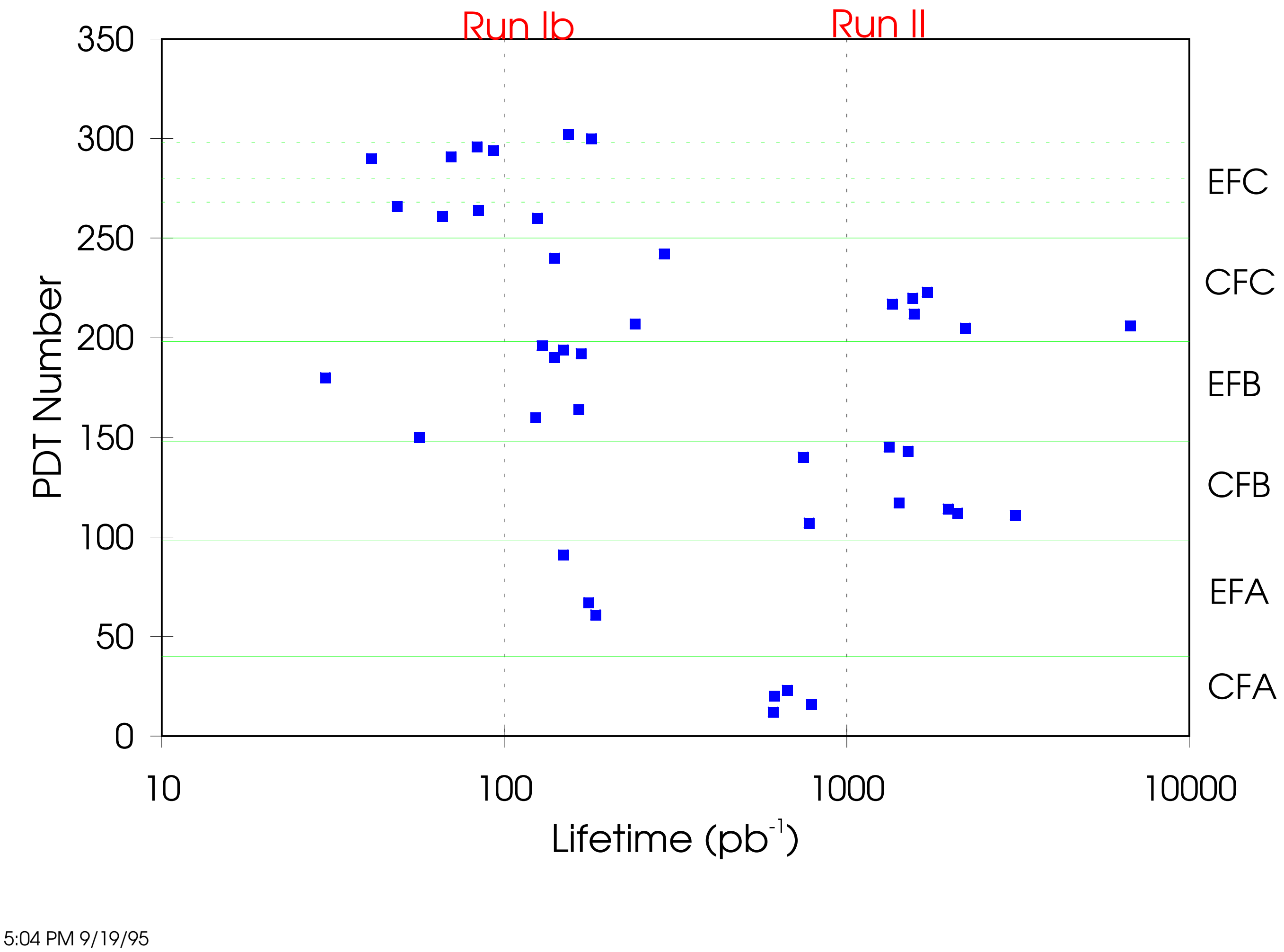

Figure 7: "Lifetime" of WAMUS PDTs versus chamber number. The approximate corresponding region is shown on the right hand axis. (EF=forward; CF=central; Letters A,B,C refer to the three stations before and after the toroid.

jets is essentially the same as those from W's so the same efficiency gains are realized for μ-tagging. Similarly, the acceptance rises from 35% to 75% for WW events. Another physics topic of interest for Run II is the measurement of the W and Z asymmetry. The W asymmetry is a crucial component in reducing the systematic error on M_W. Figure 9 shows the experimentally measured quantity, the decay-lepton charge asymmetry, as a function of $|\eta^{lepton}|$ for two popular parton distribution functions [9]. Also shown in Fig. 9 is the significance of the difference between the predictions for the two pdf's as a function of $|\eta|$ coverage. It is evident that the significance rises rapidly with $|\eta^{max}|$ up to $|\eta| \sim 2$ after which the gains are small. It is clear from these representative processes that $|\eta|$ coverage to ~ 2 is sufficient for high p_T physics. The new baseline design features full muon coverage for $|\eta| \lesssim 2$.

The muon trigger in Run II will combine track candidates from the fiber tracker trigger (CFT) with information from the muon system. The effective η range of this trigger is thus

3 The Muon System

The upgrade of the DØ muon system to permit improved triggering at high luminosity was originally presented in 1990, and approved in 1991. In this section we describe the implementation of the upgraded muon system based on our better understanding of the performance of the present muon system.

3.1 Introduction

The upgrade of the DØ muon system for Run II was last reviewed at the April 1995 PAC meeting [4]. At that time, the muon upgrade consisted of the existing Wide Angle Muon System (WAMUS) Proportional Drift Tubes (PDTs) with new electronics and a new forward trigger system made up of scintillator pixels and pad chambers. Since that review, the design of the upgraded muon system has undergone a major evolution. The primary reason for the change is the aging of the WAMUS PDTs. The chambers suffer from a radiation-induced buildup of material on the anode wires derived from the cathode pad polyresin material. This cladding can be driven off the wire by applying a short-duration high voltage pulse to the wire (called "zapping") which restores the wire gain to its original value.

Studies of the aging of the forward WAMUS chambers (the "EF" PDTs) reveal that these chambers will not survive Run II [5]. This conclusion results from consideration of Fig. 7 where the luminosity which reduces the wire gain by a factor of $1/e$ is plotted for various groupings of chambers [6]. We can define PDT "lifetime" as this luminosity and stipulate that the chamber must be 'zap cleaned' [7] after one lifetime. For example, Fig. 7 shows that the EF B-layer PDTs (EFB) must be zapped $\sim 10-20$ times during a Run II of a few fb^{-1}. Past experience with the time-consuming and difficult zapping operation has shown that a long shutdown is necessary to clean the forward chambers. Given that these shutdowns occur only several times during the course of the run, we conclude that PDTs which require zap-cleaning more than $\sim$ three times during Run II are not usable. All EF chambers are in this category. The bottom line from the aging studies is that the forward WAMUS PDTs will have to be replaced in order to retain coverage beyond $|\eta| \approx 1$.

Most of the hits in the forward muon detectors are due to remnants of hadronic and electromagnetic showers around the beam pipe [24, 25, 26]. Major improvements in the detector operation, reduced aging, trigger rates and fake track reconstruction probability can be achieved by additional shielding in the region of the beam pipe [12, 16, 24, 26]. Indeed, the most forward PDTs in the central region (CF) the so-called "ring" chambers will require a shielding factor of $\gtrsim 3$ just to survive.

In light of this, a new baseline design for the upgraded muon system has been developed. The new design was driven by the DØ Run II physics goals. The physics motivations for going to the highest luminosities are to study low-cross-section, high-p_T processes, such as top and W/Z, and to search for new phenomena. In order to maximize the acceptance for muons from these processes, we need sufficient detector coverage and an efficient, unprescaled trigger.

The range in $|\eta|$ for muons from top and WW events is shown in Fig. 8 [8]. Increasing the $|\eta|$ coverage from 1.0 to 1.7 increases the geometric detection efficiency from 50% to 85% for muons from W decay in top events. The $|\eta|$ distribution of muons from b-tagged

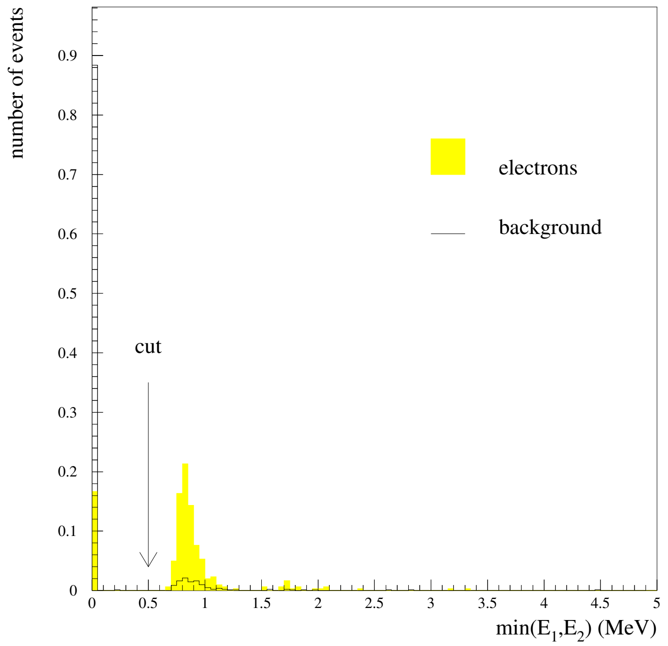

Figure 5: Minimum of energies in layers 1 and 2 for electrons from b decays and background clusters.

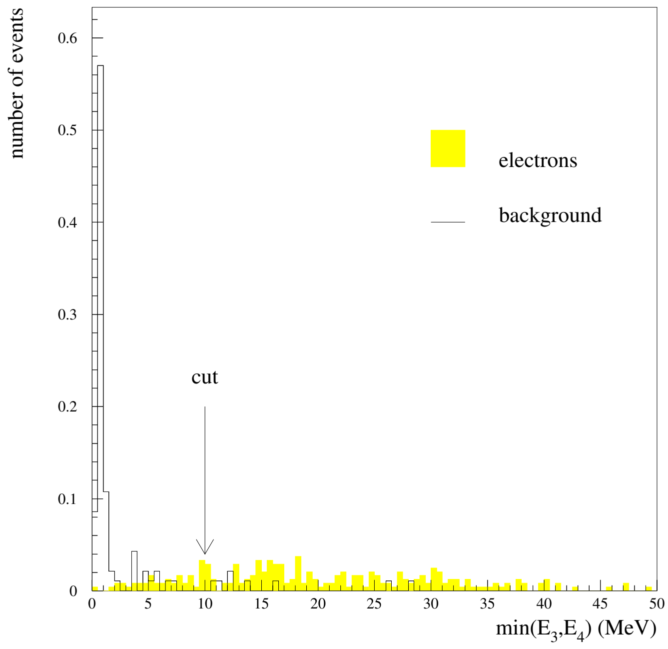

Figure 6: Minimum of energies in layers 3 and 4 for electrons from b decays and background clusters.

sample	signal	background
# of clusters	300	808
with charged track	250	94
with shower	205	9
efficiency	70%	
rejection		99%

Table 4: Efficiency and rejection for offline algorithm.

layers 1 and 2, indicating an incident charged track that points to the calorimeter cluster. We require at least 10 MeV ($\approx$ 10 mips) in layers 3 and 4 to ensure that the track started to shower in the lead absorber.

The efficiency of this simple algorithm is given by the fraction of clusters in the signal sample that are accepted. We use clusters that are due to electrons, as verified using the ISAJET information, to determine the efficiency. The rejection against background clusters is given by the fraction of clusters in the background sample that are rejected by the algorithm. Table 4 lists the results. Figure 5 shows the smaller of the layer energies before the lead for the two samples and Fig. 6 shows the smaller of the two layer energies after the lead. The algorithm rejects 99% of all background clusters, while accepting 70% of the electron clusters.

Though this study is simple and preliminary, the rate of false electron tags is $\sim$ 1%, comparable to that achieved in Run I.

2.7 Conclusions

We have performed studies of the potential benefit of a Forward Preshower Detector, covering the region $1.4 < |\eta| < 2.6$ in pseudorapidity, for the upgraded DØ detector. The region $1.65 < |\eta| < 2.5$ was assumed to consist of a 2 X_0 thick lead absorber sandwiched between two pairs of scintillator planes, which are segmented in 5 mm wide strips with a 22.5° stereo angle between the two planes in each pair. Only one pair of scintillator planes extends into the region $1.4 < |\eta| < 1.65$ where the magnet coil acts as the absorber. The total channel count for this geometry is $\approx$ 13,000. The FPS detector construction is similar to that of the Central Preshower.

We conclude that a trigger algorithm based on the energy deposited in the scintillator planes can reduce the trigger rate for isolated 20 GeV electrons in the forward region by a factor 2–3 out of Level 1 and, with inclusion of a spatial match with EM calorimeter trigger towers, by an additional factor of 3–5 after Level 2, which is insensitive to the luminosity.

We have shown that the forward preshower has the potential of substantially reducing the background to electrons from b decays in the forward region. This will be useful for b tagging in t decays as well as for b physics.

A rough estimate of the cost of the two detectors, based on the cost estimate of the Central Preshower Detector, is $\sim$\$900k.

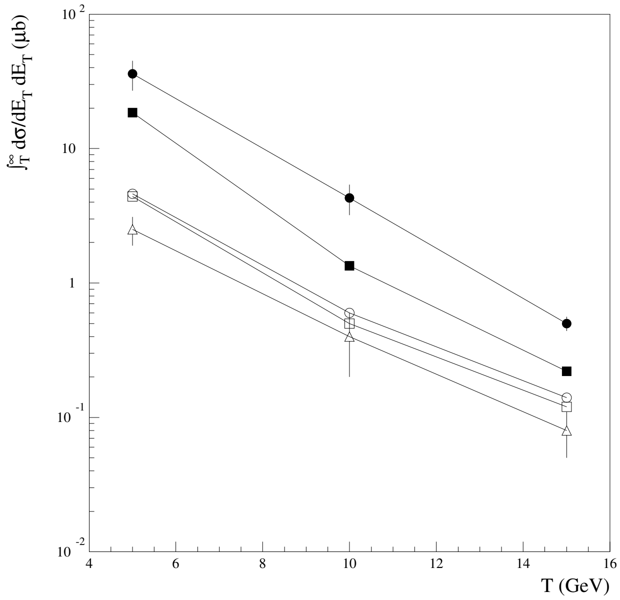

Figure 4: Trigger cross sections versus Level 1 EM trigger tower E_T threshold T. Errors are only shown on the sets of points with the highest and lowest cross sections. The FPS conditions for the five sets of points correspond to the five rows in Table 3.

cm or by eliminating the track stub detector in front of the converter. Increasing the strip width reduces the rejection by 20%, while eliminating the planes before the lead reduces the rejection by 40%. We also studied increasing the segmentation in azimuth to 32 wedges (25088 channels) and found that the rejection is improved by only 10%. We conclude that the proposed geometry is more or less optimal.

2.6 Offline Identification of Electrons

After offline event reconstruction, the event vertex and the position of EM showers in the calorimeter will be known with high precision, allowing a much tighter match between calorimeter and FPS than at the trigger level. We have performed a study of the improvement in background rejection due to the FPS information, for electrons from b decays.

As signal sample we use 508 $p\overline{p} \to b\overline{b}$ ISAJET events with $5 < p_T(b) < 20$ GeV, in which the b quarks were forced to decay to $e\nu c$. As a background sample we use 808 ISAJET dijet events with $2 < p_T(jet) < 100$ GeV. Both samples were processed through GEANT to simulate the detector response.

We start with energy clusters that are reconstructed in the electromagnetic section of the End Calorimeters. The cluster p_T must be at least 1.5 GeV (it is typically 2–3 GeV for the two samples used). We only accept clusters for which the line connecting the shower centroid with the event vertex passes through the FPS detector. We then cut on the energy deposited in the three adjacent FPS segments in each layer that are closest to this line. We require energy deposits consistent with one minimum ionizing particle (mip) or greater in

E_{iso}	Location of trigger tower	EM trigger tower thresholds		
		$T = 5$ GeV	$T = 10$ GeV	$T = 15$ GeV
none	anywhere	36. ±9. μb	4.3±1.1 μb	0.50±0.06 μb
none	EC	18.5±2.9 μb	1.34±0.32 μb	0.22±0.04 μb
∞	EC	4.6±0.7 μb	0.6 ±0.2 μb	0.14±0.03 μb
15 MeV	EC	4.4±0.7 μb	0.5 ±0.2 μb	0.12±0.02 μb
15 MeV	matched to FPS	2.5±0.5 μb	0.4 ±0.2 μb	0.08±0.03 μb
the following rates are for events with 3 additional minbias interactions				
∞	EC	10.7±2.2 μb	0.87±0.26 μb	0.14±0.10 μb
15 MeV	EC	10.5±2.2 μb	0.72±0.20 μb	0.14±0.10 μb
15 MeV	matched to FPS	2.7±0.9 μb	0.47±0.44 μb	0.11±0.10 μb

Table 3: Trigger cross section for different FPS algorithm parameters E_{iso} and EM trigger tower thresholds T.

ISAJET/GEANT in bins of jet p_T [3]. To estimate the effect of multiple interactions we give results for two-jet events containing only one interaction and for events containing an additional three soft interactions.

Table 3 lists the trigger cross sections for different FPS trigger algorithms and calorimeter EM tower thresholds for two-jet events with $10 < p_T < 500$ GeV and a single interaction. Figure 4 shows the cross section as a function of calorimeter EM tower threshold for different FPS conditions.

The first row in Table 3 lists the Level 1 cross section for an inclusive EM trigger. In order to give a useful estimate of the reduction in cross section due to various FPS trigger algorithms, we restrict the Level 1 calorimeter trigger to the ECs. In order to get the absolute trigger rate for the full acceptance of the detector, the rate for central electron triggers has to be added with corrections for overlaps between the two fiducial regions. The next three rows list cross sections for EM triggers in EC only. Row two is the Level 1 cross section for events with an EM trigger tower above threshold in EC; row three in addition requires the FPS energy term and row four the FPS isolation term. At the output of Level 1 the FPS reduces the rate for electron triggers in EC by a factor 2.3. The fifth row includes the spatial match with the EM trigger tower and the numbers in Table 3 show that at the output of Level 2 the rate is reduced by about a factor 3–5, depending on the calorimeter threshold. The last three rows give the rates for dijet events with an additional three minbias interactions superimposed. We see that the rates out of Level 1 approximately double for low thresholds, while the rate out of Level 2 for higher thresholds increases only slightly.

The FPS performance meets our goals for rejection of false electron triggers.

2.5.3 Segmentation Studies

Since the cost of the detector depends on the number of channels, we give results for geometries with different channel counts. The standard configuration requires 12544 readout channels. We can reduce the channel count drastically by increasing the strip width to 1.5

E_{iso}	Single electrons			$Z \rightarrow ee$
	$p_T = 5$ GeV	$p_T = 20$ GeV	$p_T = 50$ GeV	
∞	0.67±0.02	0.90±0.01	0.95±0.01	0.88±0.02
15 MeV	0.67±0.02	0.90±0.01	0.93±0.01	0.85±0.02

Table 2: Trigger efficiency for different electron samples.

- *isolation*: little energy in scintillator segments surrounding the segments hit by the electron.

We define a trigger algorithm for electrons which exploits all these features. The Level 1 FPS trigger requires a spatial match of preshower hits in each layer behind the lead with the corresponding track stubs in each layer before the lead. Matching a track stub two strips wide before the lead with a single strip above a threshold of 14 MeV after the lead defines a triggering algorithm with 90% efficiency, approximately independent of position, for electrons with $p_T = 20$ GeV. (Behind the magnet, the threshold is 6 MeV.)

The trigger efficiency depends on the electron energy because the track multiplicity in the preshower increases with the energy of the incident electron. Table 2 lists the efficiency of the trigger algorithm for MC samples of electrons with different p_T values. We also measure the efficiency of this trigger for electrons from $Z \rightarrow ee$ decays. This sample consists of fully simulated $Z \rightarrow ee$ decays. We select events in which exactly one of the decay electrons is reconstructed in the EC calorimeter with $1.5 \leq |\eta| \leq 2.5$ for the hottest tower.

To test whether an electron is isolated, we sum the energy deposited in a number of strips around the strips occupied by the electron shower. A high p_T electron typically deposits substantial energy in up to seven adjacent strips. We use three strips on either side of these seven strips to measure the degree of isolation and require that the energy in them is below a given limit to trigger on isolated electrons. This condition is somewhat more complicated than the condition on the energy deposits above, but it should be possible to implement at Level 1. We choose $E_{iso} = 15$ MeV, which is 85–90% efficient for electrons from Z decays (see Table 2). This efficiency is unchanged for a sample of Z events superimposed on three additional minbias interactions.

Finally, we require that the preshower trigger candidate is coarsely matched to a trigger tower in the EM calorimeter with $E_T > T$. We match any FPS trigger in an azimuthal wedge with the corresponding (η, ϕ) calorimeter trigger tower behind it. Each wedge covers two calorimeter trigger towers in azimuth and six trigger towers in pseudorapidity. This match is 100% efficient for electrons, modulo the Level 1 trigger turn-on in p_T. This condition can only be implemented at Level 2, because no information on the location of the EM trigger towers is available at Level 1.

2.5.2 Jets

We determined trigger cross sections from two-jet events which dominate the cross section for inclusive electron triggers. We used the standard two-jet samples generated with

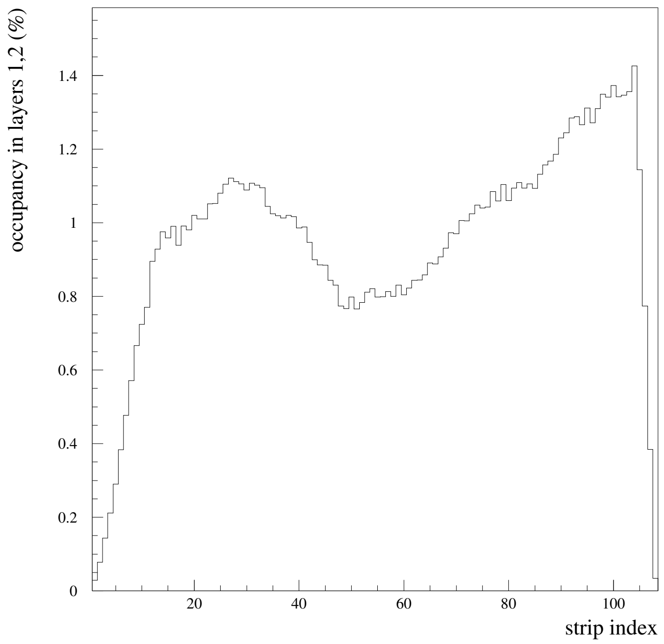

Figure 2: Occupancy of strips in scintillator layers 1 and 2.

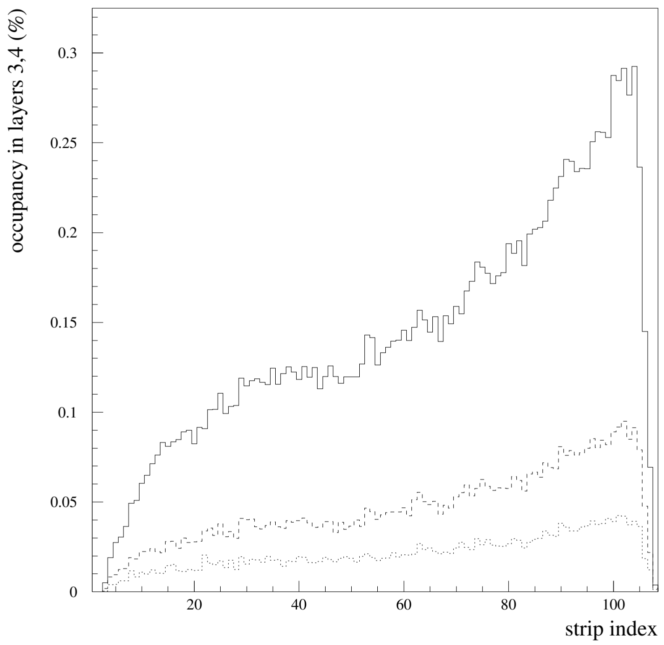

Figure 3: Occupancy of strips in scintillator layers 3 and 4 for signals with energy above 5 (——), 10 (- - -), and 15 MeV (......).

η	X_0	λ_0
1.5	2.9	0.7
2.0	0.25	0.12
2.5	0.1	0.03

Table 1: Material traversed by tracks originating from the center of the detector with pseudorapidity η.

pipe, the silicon vertex detector (SVX), and part of the scintillating fiber tracker before reaching the FPS. Tracks with $|\eta| < 1.65$ also traverse the cryostat and coil of the solenoid magnet. Table 1 lists the amount of material traversed in radiation lengths (X_0) and nuclear collision lengths (λ_0) for tracks at different pseudorapidities η [2].

Clearly, the region that is obscured by the magnet ($1.4 < |\eta| < 1.65$) is substantially different from the rest ($1.65 < |\eta| < 2.6$) of the FPS because of the large amount of material in the magnet. For $1.4 < |\eta| < 1.65$ the lead converter is not needed and should be removed or reduced in thickness in such a way that the amount of material traversed is roughly independent of η. To approximate this in our simulation we use only the scintillator layers in front of the lead converter for this region.

2.4 Occupancy

We determine the occupancy of the strips from Monte Carlo two-jet events with $10 < p_T < 500$ GeV. Figure 2 shows the probability that a strip in layers 1 or 2 has a signal above pedestal versus strip index. The enhancement in the occupancy at lower strip indices is due to particles that traverse the magnet and start showering before reaching the FPS. Figure 3 shows the probability that a strip in layers 3 or 4 has a signal with energy above 5, 10, or 15 MeV. Occupancies before the lead are about 1%.

2.5 Trigger Performance

2.5.1 Electrons

The signature of an isolated high p_T electron that traverses the FPS has the following features:

- *track stub*: an energy deposit corresponding to a single track in the scintillator layers before the lead converter.
- *preshower*: a large energy deposit corresponding to many tracks in the scintillator layers behind the lead converter.
- *match with EM calorimeter*: large energy deposit in the EM calorimeter tower behind the struck FPS element.

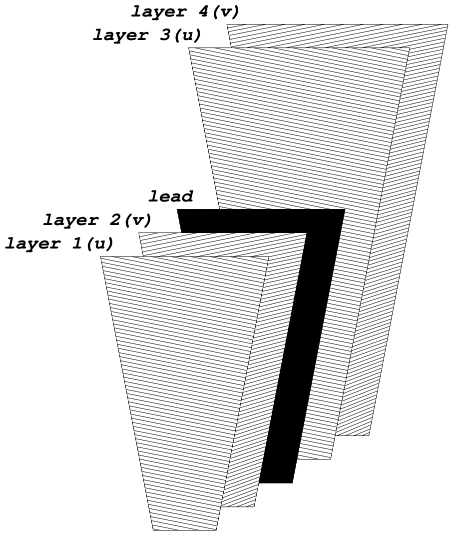

Figure 1: Schematic picture of one azimuthal wedge.

oriented perpendicular to one of the sides of the wedge, as shown in Figure 1. The orientation of the strips alternates between scintillator layers. We call the two orientations u and v layers. The size of the strips varies slightly to make the geometry projective, so that any track that originates from the center of the interaction region traverses the same segment in both u layers and in both v layers. Adjacent wedges are offset to provide room to extract the fibers. We number the scintillator layers from 1 to 4, starting with the layer closest to the interaction point.

This geometry requires a total of $108(\text{strips}) \times 16(\text{wedges}) \times 4(\text{layers}) \times 2(\text{disks}) = 13,824$ readout channels. Since the converter and the two layers of scintillator before it have no function for the region behind the magnet, the first 20 strips can be omitted for two of the scintillator layers which reduces the channel count to $12,544$.

2.3 FPS Performance

We have implemented the FPS in a GEANT simulation as disks perpendicular to the beam pipe rather than a shape that fits snugly against the EC cryostats. The inner radius of the disks is 21.1 cm ($\eta = 2.6$) and the outer radius is 74.3 cm ($\eta = 1.4$). An FPS disk consists of a lead converter, and planes of scintillator (two on either side of the converter). For each track that traverses a scintillator plane, the energy loss and the coordinates of the point at which the track crossed the scintillator are determined. There are two such disks centered at $z = \pm 141.4$ cm.

Tracks that originate from the center of the interaction region must traverse the beam

2 The Forward Preshower Detector

2.1 Introduction

The Forward Preshower Detector (FPS) will enhance the capabilities of the upgraded DØ detector for many physics topics:

- reduced trigger rates and improved offline identification for electrons in the forward region ($W \rightarrow e\nu$, $Z \rightarrow ee$, $t\bar{t} \rightarrow e + X$, $\tilde{W}\tilde{Z} \rightarrow eee$, $J/\psi \rightarrow ee$),
- improved identification of nonisolated electrons (b tagging),
- γ-π^0 separation (prompt γ production, $W + \gamma$, $Z + \gamma$).

An FPS will be located in front of each End Calorimeter (EC) and will consist of a lead converter sandwiched between two finely segmented charged particle detectors. The detector before the lead converter registers the position of charged particles from the interaction. Photons and electrons shower in the converter and the detector behind the converter detects the charged particles in the shower. Heavier charged particles like hadrons or muons will traverse the converter without showering most of the time .

We can therefore identify electrons in the FPS by requiring a large energy deposit in the detector behind the converter and a spatially matched hit in the detector before the converter. We reject photons from π^0 decays because they are not detected before the lead and charged hadrons because they do not deposit as much energy behind the lead. The dominant backgrounds for the electron signature are photons that converted before the FPS and hadrons that either interacted hadronically in the converter, creating a shower of secondaries, or overlap spatially with a photon.

The charged particle detectors must thus have the following properties: a minimum ionizing signal must be well separated from pedestal in the detector in front of the converter, the detector behind the converter must provide a pulse height measurement; both must have good spatial resolution. The signals from the detectors should be available quickly enough to be used in a Level 1 trigger. In addition, there should be as little material in front of the FPS as possible to minimize the probability of photon conversions, and the thickness of the converter in nuclear interaction lengths should be as small as possible to minimize the probability for hadrons to shower. Possible technology choices considered for these detectors included cathode pad chambers and scintillator strips with wave length shifting fiber readout.

2.2 FPS Geometry

The detection method we have chosen is to use scintillator strips with embedded wave-length-shifting fibers, read out by VLPCs. With this approach, the detector can be made to conform to the convex EC cryostats to minimize the space occupied in this crowded region. Further, by adopting this approach (which is also used for the Central Preshower), the integration of the central and forward regions is enhanced. For example, the front-end and trigger electronics are identical.

There are two planes of scintillator before the lead and two after it. Each plane consists of sixteen wedges. Each wedge is divided into 108 parallel strips, each ≈ 5 mm wide and

1 Introduction

In early 1995, the DØ Upgrade was endorsed by the Physics Advisory Committee, and a baseline cost established by a Director's Review. Since those reviews, we have attained a better understanding of three elements of the DØ Upgrade; the forward preshower system, the muon system, and the Level 2 trigger. In this document, we present the status of the designs of these three systems. These designs do not change the scope of the DØ upgrade presented in early 1995 but do increase the baseline cost estimate. Some of this information on the designs and preliminary costs were presented at the October 1995 PAC meeting.

The forward preshower design has benefited significantly from detailed Monte Carlo studies that were completed in 1995, allowing us to establish the fundamental specifications for this detector. With these specifications we have a much better understanding of the performance and costs for this system.

The muon system design has undergone a major evolution from what has been presented earlier because we have since established that the present muon proportional drift chamber system performance, particularly in the forward region, will deteriorate unacceptably for Run II. These conclusions are based on analyses, presented at the 1995 Aspen PAC, which show aging at Run I luminosities. Studies carried out over the last year have established the need for significant shielding in the forward region to control trigger rates and have had an impact on the design and costs. The resulting design involves replacement of the forward chambers, restriction of small angle coverage, and introduction of substantial shielding.

The Level 2 trigger system, a longstanding component of the DØ upgrade plan, has benefited from further simulations of expected trigger rates and the effects of multiple interactions at high luminosities. These studies have led us to conclude that we need significant computational power at Level 2 in order to achieve our trigger bandwidth goals. Detailed designs are presently under study, but all lead to cost increases beyond the baseline costs proposed in early 1995.

This document presents our current understanding of the detector capabilities needed to accomplish the physics goals established for the DØ upgrade in 1990. We seek the endorsement of the PAC of our plans for these three detector systems.

Contents

The DØ Upgrade

Forward Preshower
Muon System
Level 2 Trigger

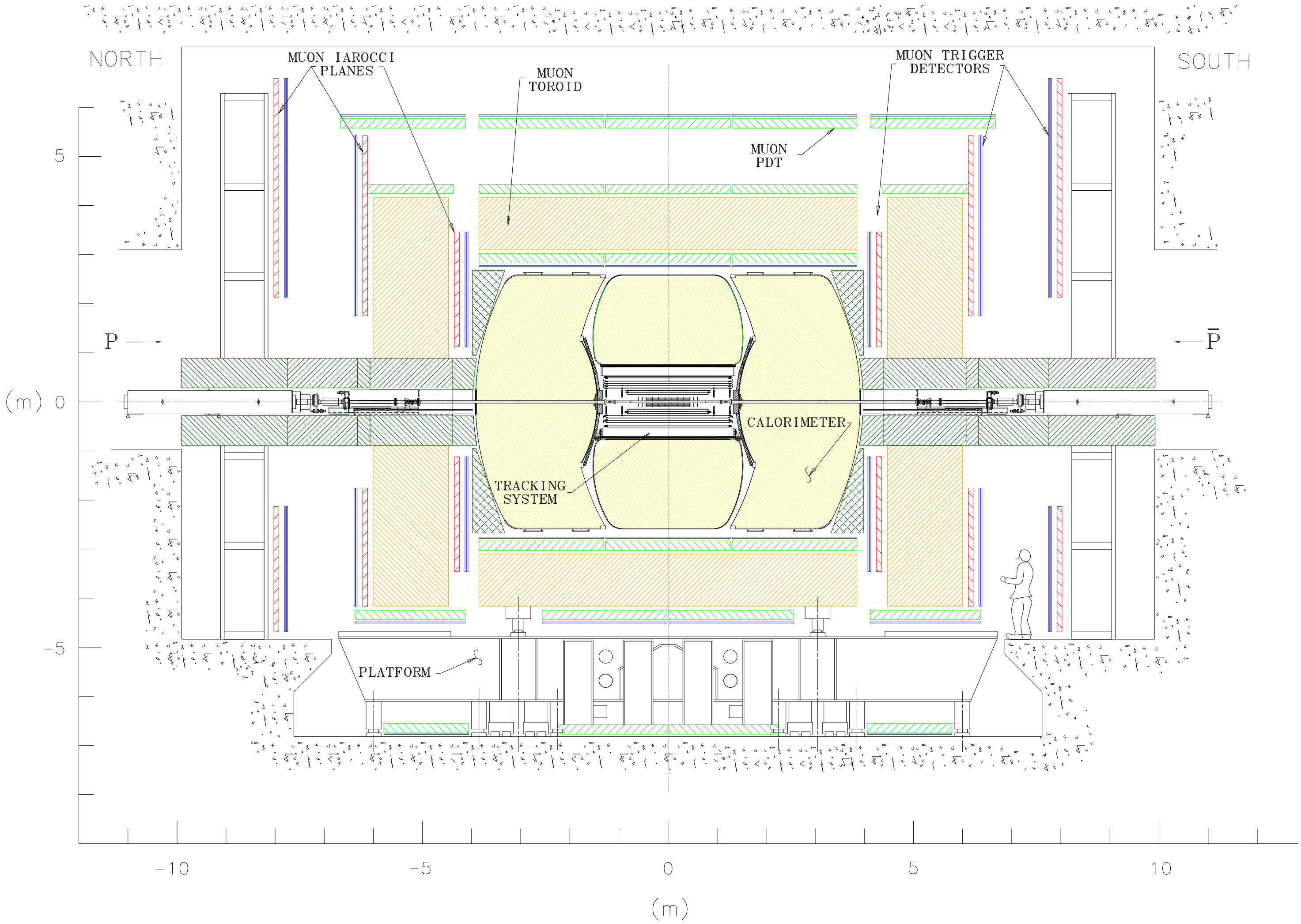

The DØ Collaboration

January 18, 1996